Electron density and collision frequency of microwave resonant cavity produced discharges.

W. McColl, C. Brooks, and M. L. Brake
Department of Nuclear Engineering, University of Michigan, Ann Arbor, Michigan, 48109-2104
(Received

A review of perturbation diagnostics applied to microwave resonant cavity discharges is presented. The classical microwave perturbation technique examines the shift in the resonant frequency and cavity quality factor of the resonant cavity caused by low electron density discharges. However, modifications presented here allow the analysis to be applied to discharges with electron densities beyond the limit predicted by perturbation theory. An 'exact' perturbation analysis is presented which models the discharge as a separate dielectric, thereby removing the restrictions on electron density imposed by the classical technique. The 'exact' method also uses measurements of the shifts in the resonant conditions of the cavity. Thirdly, an electromagnetic analysis is presented which uses a characteristic equation, based upon Maxwell's laws, and predicts the discharge conductivity based upon measurements of a complex axial wave number. By allowing the axial wave number of the electromagnetic fields to be complex, the fields are experimentally and theoretically shown to be spatially attenuated. The diagnostics are applied to continuous-wave

microwave (2.45 GHz) discharges produced in an Asmussen resonant cavity. Double Langmuir probes, placed directly in the discharge at the point where the radial electric field is zero, act as a comparison with the analytic diagnostics. Microwave powers ranging from 30 to 100 watts produce helium and nitrogen discharges with pressures ranging from 0.5 to 6 torr. Analysis of the data predicts electron temperatures from 5 to 20 eV, electron densities from 10^{11} to 3×10^{12} cm^{-3}, and collision frequencies from 10^{9} to 10^{11} sec^{-1}.

I. INTRODUCTION

Microwave resonant cavity discharges and electron cyclotron resonance (ECR) discharges have become increasingly useful in industrial processes. The low pressure, low ion energy characteristics of ECR discharges make them promising alternatives to radio frequency coupled devices in the field of plasma processing of materials. Due to the inherent use of microwaves in ECR discharges, ECR designs utilizing microwave resonant cavity discharges are being extensively studied for use in plasma processing and thin film deposition[1].

Resonant cavity discharges have many additional applications other than materials processing, such as fluorescent excimer lamp systems[2,3] and as a possible laser medium[4]. Due to the lack of electrodes, resonant cavities are very durable yet simple in design and operation. The availability of inexpensive microwave components at 2.45 GHz is also an attractive feature.

Prior to 1970, the electromagnetics of microwave resonant cavities perturbed by discharges have been extensively studied.[5-22] An article published in 1946 by J.C. Slater[5] extensively details research on microwave electronics completed during World War II at the Massachusetts Institute of Technology. The article details the effects that an arbitrary conductance places on a microwave resonant cavity. The techniques presented by Slater were then applied specifically to plasma discharges.[6-8] These initial techniques were actually used with repetitively pulsed discharges, either formed by the electromagnetic fields within the cavity or produced externally. In a series of four papers by S.C. Brown and coworkers,[9-12] the Slater technique was extensively detailed, as well as its applications as an electron density and collision frequency

diagnostic of externally produced discharges.

The Slater technique, commonly referred to as perturbation analysis, determines the shifts in the resonant conditions of the microwave cavity due to a complex conductivity present in the cavity. The real portion of the conductivity causes a shift in the cavity quality factor while the imaginary portion shifts the resonant frequency of the cavity. Discharge theory then relates the complex conductivity to the electron density and electron-neutral collision frequency.

Perturbation analysis in its original form does not address the implication the discharge places on the electromagnetic fields. When analyzing the lumped cavity-discharge circuit, the electric fields are assumed to be those of an empty cavity. In this way, the complex dielectric constant of the discharge is ignored and the discharge and resonant cavity circuit are treated by electronic circuit theory. While this simplification is justifiable for low electron density, low pressure discharges, it becomes a major source of error for high density discharges. These errors were analyzed in a paper published in 1957 by K.B. Persson,[13] where the limits of perturbation analysis are studied and details of how to slightly extend these limits are presented. In a contemporaneous publication, S.J. Buchsbaum et al.[14] demonstrated experimentally which resonant cavity modes are appropriate for high density discharges, and determined for S band microwaves the upper limit of allowable electron density, namely 10^{12} cm^{-3}.

One refinement of perturbation analysis is to include the spatial variations of the plasma discharge.[15,16] This technique was actually presented as a method to determine the spatial profile of low density discharges. However, this procedure also demonstrates a reduction of the

errors inherent to perturbation analysis.

Developed after the perturbation analysis is the so called 'exact' theory,[17-20] a method which was actually applied to wave guide discharges as early as 1947.[21,22] In this procedure, the plasma discharge is included in the resonant cavity as a separate dielectric. By matching the electromagnetic field boundary conditions along the surface of the discharge as well as at the cavity walls, a characteristic equation is obtained. Solutions of the characteristic equation provide the conductivity of the discharge as a function of the shift in the resonant frequency of the cavity. If the collision frequency is not zero, the electromagnetic fields become complex which greatly complicates the characteristic equation. The effect of electron collisions was addressed by expanding the characteristic equation solutions in a Taylor series about the zero collision frequency solutions. However, the 'exact' theory is applicable to high density discharges since the characteristic equation models the electromagnetic fields in the presence of a discharge. This is a departure from Brown's treatment of the discharge as a lumped circuit element.

The basic premise of the electromagnetic analysis presented here, similar to recently developed models,[23-26] is to model the discharge as a lossy dielectric produced in a reduced density gas channel by absorbing microwave power delivered to a surrounding resonant cavity. This departs from the perturbation analysis and the 'exact' theory since the discharge is formed by the resonant cavity fields, rather than simply placing a resonant cavity around an existing discharge. Maxwell's equations are solved in all regions of the cavity by assuming that the cavity is excited in a specific electromagnetic mode and that the forward and backward traveling electromagnetic waves have a complex axial wave

number. This is unlike previous models[17-20,23] which have assumed a real wave number but a complex microwave frequency. A complex axial wave number is required to account for the attenuation of microwaves as they propagate along the discharge, as well as the absorption of microwave power by the discharge. Details of the electromagnetic analysis are given in the following section.

Non-intrusive diagnostics, in addition to the modeling of the electromagnetic fields in the cavity, have been applied to resonant cavity discharges to measure various characteristics. These include laser induced fluorescence diagnostics[27] and emission spectroscopy studies,[28] as well as the application of a Langmuir probe directly into the discharge within the resonant cavity.[29] This paper also presents a review of classical microwave cavity diagnostic techniques and compares these with more extensive versions. The results of double Langmuir probes applied to a resonant cavity discharge are compared with cavity perturbation analyses and the electromagnetic analysis of the fields in the cavity.

II. ELECTROMAGNETIC ANALYSIS

The purpose of this analysis is to model a discharge which is created by absorption of energy contained in electromagnetic fields in a resonant microwave cavity. As the electromagnetic fields travel along the dissipative discharge, they become spatially attenuated. This type of attenuation requires a complex axial wave number while the microwave frequency is kept real and constant. The resonant cavity used in this experiment is tuned by shifting the length of the cavity, rather than by varying the microwave frequency. The mode configuration studied is a transverse magnetic (TM_{012}) mode, although this analysis may be modified

for use in other cavities and modes.

A diagram of the geometry used in the analysis is shown in Fig. 1. In the analysis, outlined in Fig. 2, the resonant cavity is divided into three regions: 1) the partially ionized discharge produced in a gas channel contained by a quartz tube, 2) the containment vessel (quartz), and 3) the free space extending from the containment vessel to the cavity walls. It is assumed that the discharge fills the vacuum vessel and that the regions are isotropic and continuous along the axis of the cavity. Electromagnetic fields based upon a TM_{012} mode are derived for the three regions using Maxwell's equations. The presence of the discharge affects both the wave number of the electromagnetic fields and the permittivity of the discharge, which become complex in value.

Boundary conditions are used to relate the electromagnetic fields at the interfaces of the different regions. These relations are used to produce a characteristic equation, the roots of which provide the electrical permittivity of the discharge. By knowing the wave number of the discharge, which is found using the length of the cavity and the attenuation of the electromagnetic fields, these roots may be determined. A model for the AC conductivity then provides the electron density and electron-neutral collision frequency. Therefore, in effect the characteristic equation provides the electron density and collision frequency based upon the attenuation of the electromagnetic fields and the shifted length of the resonant cavity.

The analysis provides the form of the field components in the three regions, but not their amplitude. The Joule heating absorbed power and the energy contained in the electromagnetic fields is used to find the amplitude of the fields. By integrating the electromagnetic fields over the

volume of the three regions, a dissipated power is found as the product of the integrals with the permittivity of each region. The amplitude of the electromagnetic fields is found by a comparison with the measured absorbed power.

Using Maxwell's equations and assuming time harmonic waves varying with frequency ω gives the Helmholtz wave equation in cylindrical coordinates[30]

$$\frac{1}{\rho}\frac{\partial}{\partial\rho}\left(\rho\frac{\partial E_{zi}}{\partial\rho}\right)+\frac{1}{\rho^2}\frac{\partial^2 E_{zi}}{\partial\theta^2}+\frac{\partial^2 E_{zi}}{\partial z^2}+k^2 E_{zi}(\rho,\theta,z)=0 \qquad (1)$$

where E_{zi} is the axial component of the electric field in the region of interest, $k=\omega\sqrt{\mu_0\varepsilon_i}$ is the wave number of the electromagnetic waves, and ε_i is the permittivity of region i. A solution of this wave equation provides a wave traveling in the +z direction in the region of interest. Solutions of a similar wave equation obtain waves traveling in the -z direction. The permittivity of the empty cavity is assumed to be ε_0 and the permittivity of the quartz glass is 3.78 ε_0.[26,30] The discharge is assumed to be a lossy dielectric with a complex permittivity given by[31]

$$\varepsilon_1=\left(\varepsilon_0+\frac{\sigma_I}{\omega}\right)-j\left(\frac{\sigma_R}{\omega}\right) \qquad (2)$$

where σ_R and σ_I are the real and imaginary components of the complex discharge conductivity, respectively.

Using the separation of variables technique, equation (1) can be used to determine E_{zi}^+, the axial component of the electric field in region i traveling in the forward direction. A similar solution is found for E_{zi}^-, the

reflected wave. Note that in a transverse magnetic mode, $B_{zi}^{\pm}\equiv 0$. The remaining fields are then calculated using Maxwell's equations and $E_{zi}^{\pm}$. To satisfy boundary conditions, the amplitude of the forward and reflected waves must be equal. A superposition of the two traveling waves in a TM_{012} mode gives the electromagnetic fields for region i as:

$$E_{\rho i}(\rho,\theta,z,t) = \frac{k_z}{k_{\rho i}}\exp\{j\omega t\}[\cosh\{\alpha z\}\sin\{\beta z\} - j\sinh\{\alpha z\}\cos\{\beta z\}]\left[A_i J_1(k_{\rho i}\rho) + B_i Y_1(k_{\rho i}\rho)\right] \quad (3a)$$

$$E_{zi}(\rho,\theta,z,t) = \exp\{j\omega t\}[\cosh\{\alpha z\}\cos\{\beta z\} - j\sinh\{\alpha z\}\sin\{\beta z\}]\left[A_i J_0(k_{\rho i}\rho) + B_i Y_0(k_{\rho i}\rho)\right] \quad (3b)$$

$$B_{\theta i}(\rho,\theta,z,t) = \frac{j\omega\mu_0\varepsilon_i}{k_{\rho i}}\exp\{j\omega t\}[\cosh\{\alpha z\}\cos\{\beta z\} - j\sinh\{\alpha z\}\sin\{\beta z\}]\left[A_i J_1(k_{\rho i}\rho) + B_i Y_1(k_{\rho i}\rho)\right] \quad (3c)$$

$$E_{\theta i}(\rho,\theta,z,t) = 0 \quad (3d)$$

$$B_{\rho i}(\rho,\theta,z,t) = 0 \quad (3e)$$

$$B_{zi}(\rho,\theta,z,t) = 0 \quad (3f)$$

where

$$k_z = \beta - j\alpha \equiv \textit{axial wave number} \quad (4a)$$

$$k_{\rho i} = \sqrt{\omega^2\mu_0\varepsilon_i - k_z^2} \equiv \textit{radial wave number} \quad (4b)$$

Here, one cavity end wall is placed at z=0 while the other is at z=L. In the axial wave number, the quantity β leads to harmonic fields in the axial direction while α is an attenuation constant which accounts for power being absorbed by the discharge. For a TM_{012} mode, β is given by $2\pi/L$, where L is the length of the resonant cavity. Note that $k_{\rho l}$ in equations (3) and (4) is complex, due to the complexity of k_z. Thus, the arguments of the Bessel's functions in equations (3) become complex as do the coefficients A_l and B_l.

Boundary conditions are now used to relate the fields at the interfaces of the regions. The coefficients of the fields (A_l and B_l) are eliminated, producing a characteristic equation (see Appendix). This equation is then used to calculate the conductivity of the discharge. These boundary conditions are:

a) the fields are finite

b) any electric field lying parallel to a cavity wall goes to zero at the wall

c) E_z and B_θ are continuous at a region interface

The second boundary condition stems from the assumption that the cavity walls are perfectly conducting. The third boundary condition follows from Faraday's and Ampere's law.[30]

Due to the second boundary condition, the radial electric field should be equal to zero at both ends of the cavity, i.e. at z=0 and at z=L. Two waves will add to zero only if the waves have equal magnitude, an assumption already made in equations (3). This also requires that the quantity β must be an integer multiple of π/L while the quantity α must be

zero, i.e. the axial wave number must be completely real.

Past studies have remained true to this condition by ignoring any spatial attenuation of the electromagnetic fields. This requires that the microwave frequency be complex, while maintaining a real axial wave number. A complex frequency leads to temporally damped fields, while a complex axial wave number provides spatially attenuated fields. Spatial attenuation implies a reference point from which the fields are attenuated, even though it has been assumed that the cavity is symmetric. Therefore, in a perfectly symmetric cavity there can be no spatial attenuation.

In practice, however, there is spatial attenuation of the electromagnetic fields. The reason for this is simple: in practice the cavity is not perfectly symmetric. The reference point for this asymmetry is the port or antenna from which the microwaves are launched into the cavity, as illustrated in Fig. 1. To account for this asymmetry, the cavity is broken into two regions in the axial direction: 1) region X which extends from one cavity wall to the microwave coupling antenna ($0<z<L_{ant}$), and 2) region Y which extends from the antenna to the other cavity wall ($L_{ant}<z<L$). The boundary conditions are met by assuming that the radial electric field is zero at $z=0$ in region X and at $z=L$ in region Y, while continuous at the interface at $z=L_{ant}$. Solutions based upon this assumption still satisfy Maxwell's equations as well as equation (1) and are presented in the Appendix. A spatially attenuated standing wave is shown in Fig. 3 as well as samples of the radial electric field taken at the wall of the cavity using an electric field probe, which verifies that the attenuation is a spatial phenomenon. The electric field probe samples the square of the magnitude of the radial electric field at various positions along the length of the cavity.

The characteristic equation is a complex equation, the roots of which provide the conductivity of the discharge as a function of the axial wave number, calculable from experimental data. Discharge theory provides a theoretical model of the conductivity for comparison with the solutions of the characteristic equation. If the electron-neutral collisions are elastic and the distribution function is uniform, the conductivity becomes[31]

$$\sigma = -\frac{4\pi}{3}\frac{e^2}{m_e}\int_0^\infty \frac{v^3 \frac{\partial f_0}{\partial v}}{\nu(v)+j\omega}dv \tag{5}$$

where f_0 is the first term of an expansion of the electron distribution function and $\nu(v)$ is the electron collision frequency. Typically, $\nu(v)$ for different gases is a function of the electron velocity v and equation (5) becomes a function of the electron distribution f_0. To overcome this dependence, an effective collision frequency may be defined as[31,32]

$$\nu_{eff} = \frac{\int_0^\infty v^3 \frac{\nu(v)}{\nu(v)^2+\omega^2}\frac{\partial f_0}{\partial v}dv}{\int_0^\infty v^3 \frac{1}{\nu(v)^2+\omega^2}\frac{\partial f_0}{\partial v}dv} \tag{6}$$

Using this effective collision frequency, the conductivity becomes

$$\sigma = \sigma_R + j\sigma_I \tag{7a}$$

$$\sigma_R = \frac{n_e e^2}{m_e}\frac{\nu_{eff}}{\left\{(\nu_{eff})^2+\omega^2\right\}} \tag{7b}$$

$$\sigma_I = -\frac{n_e e^2}{m_e} \frac{\omega}{\left\{(\nu_{eff})^2 + \omega^2\right\}} \tag{7c}$$

Once the conductivity is found using the characteristic equation, it can be substituted into equations (7) and the electron density and effective electron collision frequency may be determined.

The time averaged power dissipated is found by

$$P_D = \frac{1}{2}\Re e\left\{ \int_{plasma} \bar{E} \bullet \left(\sigma \bar{E}\right)^* dV \right\} + \sum_i \int_{region\,i} \frac{\omega}{Q} \varepsilon_i \left|\bar{E}_i\right|^2 dV \tag{8}$$

The first term represents a Joule heating term of the discharge while the second term represents the energy stored in the electromagnetic fields in the three regions and dissipated in the cavity walls. The electric fields are known to within a constant, their amplitudes A_i and B_i. By use of the boundary conditions, these coefficients may be related to A_1. The electric fields, conductivity and permittivities may then be integrated over the cavity leaving a value multiplied by the square of the amplitude of the electromagnetic fields, $|A_1|^2$, the product of which provides an absorbed power. This power is now compared with the measured input power, and the coefficient $|A_1|$ is adjusted until the two powers match. Once this is completed, the magnitude of all of the electromagnetic fields throughout the microwave cavity may be calculated.

III. CAVITY PERTURBATION

A. Classical Perturbation Technique

Microwave cavity perturbation diagnostics depend upon the

conductivity of the discharge in question to detune the resonant cavity. By measuring the amount of detuning, both the electron density and the electron collision frequency may be determined. The shift in the resonant conditions is given by[5]

$$\Delta\left(\frac{1}{Q}\right)-2j\frac{\Delta\omega}{\omega}=\frac{1}{\varepsilon_0\omega}\frac{\int_{plasma}\bar{J}\bullet\bar{E}_0dV}{\int_{cavity}\bar{E}\bullet\bar{E}_0dV} \tag{9}$$

where J represents the current density and E represents the electric fields present within the cavity. All of the integrals are over volume, V. The subscript '0' refers to conditions in the cavity without a discharge present. The shift in the resonant frequency of the cavity caused by the discharge is $\Delta\omega$ and Q is the cavity quality factor.

The electric fields present in an unloaded cavity are given by[30]

$$E_{\rho 0}(\rho,\theta,z)=\frac{2\pi/L}{\sqrt{\omega^2\mu_0\varepsilon_0-\left(2\pi/L\right)^2}}J_1\left(\rho\sqrt{\omega^2\mu_0\varepsilon_0-\left(2\pi/L\right)^2}\right)\sin\left(2\pi\frac{z}{L}\right) \tag{10a}$$

$$E_{z0}(\rho,\theta,z)=J_0\left(\rho\sqrt{\omega^2\mu_0\varepsilon_0-\left(2\pi/L\right)^2}\right)\cos\left(2\pi\frac{z}{L}\right) \tag{10b}$$

$$E_{\theta 0}(\rho,\theta,z)=0 \tag{10c}$$

Typically, Ohm's law is used to represent the current density (i.e. $J=\sigma E$, where the conductivity σ is given by equations (7)) and the real and imaginary components of equation (9) provide calculations of the electron density and effective collision frequency.

Generally, perturbation techniques are not applicable to high density ($n_e > 5\times10^9$ cm^{-3}) discharges.[13] For low density discharges, the plasma frequency is much less than the microwave frequency and the effect of the discharge on the electric fields is small. In this case, $E \bullet E_0$ is replaced by E_0^2. That is, the electric fields in the presence of the discharge are approximately the same as those of an unloaded cavity. As the plasma frequency approaches the microwave frequency, this is less likely the case and the errors involved become intolerable. However, it has been shown[13,14] that in certain cases densities up to 10^{12} cm^{-3} may be accurately measured with this technique. In particular, if the electric fields lie perpendicular to any electron density gradients the technique can be used at high densities. The phrase 'classical perturbation' will be used to designate the use of $E \bullet E_0 = E_0^2$ in equation (9).

Measuring the cavity Q in the presence of a discharge is a difficult and inaccurate process. To do this requires the superposition of a variable frequency microwave signal with the fixed frequency CW signal and sweeping the frequency while monitoring any reflected signal. This may be accomplished using various experimental configurations. However, the reflected CW signal usually overwhelms any reflections due to the variable frequency signal, resulting in a very poor signal-to-noise ratio. To overcome this the definition of the cavity Q, given below, is utilized.[30]

$$Q = \omega \frac{\textit{energy stored}}{\textit{energy dissipated}} \qquad (11)$$

The energy stored is simply proportional to the square of the electric fields[30], measurable using a simple electric field probe. The energy dissipated can also be measured. Therefore, the cavity Q in the presence of

a discharge is approximately[26]

$$Q = Q_0 \frac{P_{T0}}{P_T} \frac{|E_{\rho w}|^2}{|E_{\rho w0}|^2} \tag{12}$$

where the subscript '0' refers to conditions in the cavity without a discharge present, P_T is the dissipated energy, and $|E_{\rho w}|^2$ represents the electric field probe measurements, typically sampled at the wall of the cavity. To measure the shifted resonant frequency, the discharge is ignited and the cavity is tuned by minimizing the reflected microwave power. The discharge is then turned off and the resonant frequency is measured without readjusting the cavity length. In this way both $\Delta\omega$ and Q can be measured and the electron density and collision frequency can be calculated.

The classical perturbation integrals in equation (9) can be calculated using the electric fields given in equations (10) by assuming that $E \bullet E_0 = E_0^2$. Since the electron density is included in the integrals, a functional form for the electron density may be included to permit integration along with the electric fields.[15,16] This is done to minimize the error of the classical perturbation technique. Since the time averaged power dissipated is proportional to the square of the electric fields, and the electron density in general follows the dissipated power, it is assumed that the electron density follows the electric fields squared (see equations (10)). Note, however, that the radial component of the electric field is close to zero at the center of the cavity where the discharge is present (due to $J_1(\rho=0)=0$), and thus may be ignored. Therefore, the electron density can be assumed to follow the square of the axial component of the electric field, or

$$n_e(\rho,z) = n_0\left\{J_0\left(\rho\sqrt{\omega^2\mu_0\varepsilon_0 - \left(2\pi/L\right)^2}\right)\cos\left(2\pi\frac{z}{L}\right)\right\}^2 \qquad (13)$$

This is further supported by fiber optic probe data, used to measure the optical emission as a function of axial position. In general, the optical emission follows $\cos^2(2\pi z/L)$. Since the electron density follows the electric field, the fields are not perpendicular to any density gradients. However, as will be shown, application of perturbation techniques to densities above 10^9 cm^{-3} is justified.

Since the discharge is not confined in the axial direction, the plasma does not always fill the entire length of the resonant cavity. The bounds of the discharge therefore run radially from $\rho=0$ to the inner wall of the vacuum vessel, and axially from some position $z=L_{start}$ to $z=L_{stop}$. The quantities L_{start} and L_{stop} are the experimentally measured physical bounds of the discharge. These are demonstrated in Fig. 4, which shows data of the light emission of a discharge. Using the functional form of the electron density given in equation (13), the integrals in equation (9) are calculated for each particular experimental situation. Combined with the complex conductivity, the real and imaginary components are equated to the shifts in the resonant frequency and cavity Q.

It is interesting to note that as the length of the discharge changes, the integral of the electric fields over the plasma volume also changes. Therefore, the proportionality constant predicted by the classical technique (i.e. $\Delta\omega = k\, n_e$) decreases with plasma volume. By including this variation in plasma length, the classical perturbation technique may yield reasonably accurate results at higher electron densities (>10^9 cm^{-3}).

B. Exact Perturbation Technique

As was shown in the previous section, it is possible to calculate solutions for the electromagnetic fields in the presence of a discharge. These solutions may then be used in equation (9), removing the conditions restricting the electron density. However, it is difficult to solve equation (9) analytically, since they involve Bessel functions of complex arguments. A derivation presented in the Appendix shows that in the presence of a discharge, the perturbation equation becomes simply

$$\int_{cavity}\left\{\overline{B}\bullet\overline{B}+\mu_0\varepsilon\overline{E}\bullet\overline{E}\right\}dV=0 \tag{14}$$

which can be solved numerically. Note that the electromagnetic fields are dotted with themselves, not with their complex conjugates, so that the dot products are not necessarily positive definite quantities. In this way the integrals of the complex Bessel functions reduce to equations which are solved using a complex root finding routine. Here the microwave frequency is allowed to be complex and shift, with

$$\omega=\omega_R+j\omega_I \tag{15a}$$

$$\omega_I=\frac{\omega_R}{2}\Delta\left(\frac{1}{Q}\right) \tag{15b}$$

Fields similar to those shown in equations (3) may be used in equation (14) for an 'exact' perturbation analysis. Unlike the classical perturbation technique, which uses a spatial electron density profile as in

equation (13), the 'exact' analysis assumes the discharge is isotropic and continuous throughout the discharge region. To analyze an electron density which varies with position, the arguments of the Bessel functions in equations (3) become functions of position which greatly complicates the 'exact' analysis.

The 'exact' theory first introduced by S.C. Brown[17] is actually an electromagnetic analysis, similar to the one presented in the previous section, since it matches boundary conditions to obtain a characteristic equation. Equation (14) is a perturbation technique, since it deals with the integration of the electromagnetic fields over the volume of the cavity. Also, in Brown's 'exact' theory, the effects of the collision frequency were ignored to ensure the electromagnetic fields remain real. The presence of a collision frequency causes the discharge permittivity to become complex and complicates the analysis. Both the electromagnetic analysis and 'exact' perturbation analysis presented here deal with the collision frequency directly, since no restrictions are placed on the collision frequency and the fields are not restricted to being completely real.

The electron density predicted by the classical and 'exact' perturbation analysis is illustrated in Fig. 5. The solid line represents solutions predicted by the 'exact' analysis. The dashed line is from the classical theory for a discharge which entirely fills the cavity, while the dashed line with circles is for a discharge which fills half the cavity, centered in the middle. Classical perturbation theory (equation (9)) predicts that the electron density varies linearly with the frequency shift, while the 'exact' analysis (equation (14)) predicts a departure from this linearity above electron densities of 5×10^{11} cm^{-3}. This agrees with the well known work of S.C. Brown, et al.[17,18] which predicts a departure

around 10^{12} cm^{-3} for a TM_{020} mode. However, the electric fields of the TM_{020} mode are completely perpendicular to any density gradients, as opposed to those of the TM_{012} mode. Also note that the classical and 'exact' perturbation method do not give precisely the same results below 5×10^{11} cm^{-3}. This is because the 'exact' technique presented here accounts for the effect of the dielectric constant of the quartz tube, while the classical treatment does not.

IV. EXPERIMENT

In this experiment, helium and nitrogen discharges were contained in a quartz tube (25mm i.d., 28mm o.d.) placed along the axis of an Asmussen[33,34] resonant cavity operating in a transverse magnetic (TM_{012}) mode. The cavity walls are constructed of brass, and therefore highly conductive. The inner radius of the cavity is 8.9 cm, but the length of the cavity may be varied from 6 to 16 cm by use of a sliding short. Variations in the cavity length are necessary because the presence of the discharge shifts the resonant conditions of the cavity. A microwave coupling antenna acts as a variable impedance transformer between the wave guide carrying the microwaves and the resonant cavity. The microwave coupling antenna is designed such that the depth at which the antenna is inserted into the cavity is variable. Both the sliding short and the coupling antenna are varied until the reflected power is minimized, typically to values less than 2% of the power supplied to the cavity. A schematic of the microwave cavity is shown in Fig. 6. Welded to one side of the cavity is a wire mesh window, permitting viewing of the discharge and optical emission spectroscopy diagnostics.

Electric field measurements are made by use of a simple electric field

probe. The electric field probe consists of a short length of micro-coaxial wire connected to a microwave power meter. The probe is inserted into small holes which run along the length of the cavity wall. It is arranged such that the inner conductor of the probe extends a few millimeters into the interior of the cavity. In this way, the probe measures a value proportional to the square of the magnitude of the radial electric field sampled at the wall of the cavity, or $|E_{\rho w}|^2$.

The microwave circuit consists of a power source, a terminated three port circulator, a bi-directional coupler and power meters, and the microwave cavity itself. Coaxial components are used throughout, with coaxial wave guides used to interconnect the components. The power source is a Micro-Now continuous wave magnetron oscillator with a fixed frequency of 2.45 GHz and adjustable power from 0 to 500 watts.

V. DOUBLE LANGMUIR PROBE

A. Experimental technique

The electromagnetic fields in a resonant cavity are easily disturbed. If metallic probes are inserted into a cavity, their placement must ensure that the electric fields are not distorted. The electromagnetic fields of an unloaded cavity operating in a TM_{012} mode were shown previously in equations (10). Due to the $\sin(2\pi z/L)$ dependence, the radial electric field at the plane $z=L/2$ is completely zero and the electric field lies only in the axial direction. It has been demonstrated[29] that if the discharge does not perturb the general shapes of the fields, then it is possible to insert thin tungsten wires into these null positions to act as Langmuir probes. In this way the electric field lies only along the diameter of the wire, and the amount of microwave power absorbed by the wires is negligible. For other

positions or orientations, the components of the electric field would lie parallel to the wire and the wire would act as an antenna, coupling the microwaves out of the cavity.

The cavity quality factor, or cavity Q, is a measure of how well a cavity stores the energy that is introduced to it. At the resonant frequency of a tuned cavity all of the incident power is absorbed by the cavity. Experimentally the resonant circuit Q is determined by[9,30]

$$Q_{circuit} = \frac{\omega_0}{\Delta\omega} \tag{16}$$

where ω_0 is the resonant frequency of the cavity and $\Delta\omega$ is the width of a swept frequency versus reflected power curve. When the cavity is tuned, the cavity Q is twice that of the resonant circuit Q.[9] In this experiment the cavity Q without the Langmuir probe wires was approximately 6500 while with the probe wires it was roughly 5000. The theoretically maximum cavity Q of the resonant cavity is 15,500.[30]

One source of error in this experiment is the measurement of the surface area of the Langmuir probe wires. The probes are affixed to the vacuum vessel using a ceramic vacuum seal, and tend to slip a small amount as the sealant dries. Once embedded, it is difficult to access the probes. The probe areas were less than 0.020 cm^2, (typically a tungsten wire, with a diameter of 0.041 cm and a length of 0.15 cm). A swept voltage circuit[29] is used for acquiring the voltage-current characteristics.

B. Double probe theory

Many papers and texts have been written on double probe theory.[35-37] The two primary values derived from double probe characteristics are

the electron temperature and the ion density. An inherent assumption to double probe theory is that the electrons of the discharge in question are described by a Maxwellian distribution. This may or may not be valid, but the assumption is the best available for the discharge described in this paper. The theory also assumes that the probe radius is larger than the electron Debye length,[35] a requirement that is met in this experiment ($\lambda_D \cong 0.003$ cm, $r_p = 0.04$ cm).

The derivation of the electron temperature used in this experiment was first presented by T. Dote.[37] The electron temperature is determined by the following

$$T_e(eV) = (0.244)\frac{I_{s1} + I_{s2}}{\left.\frac{dI}{dV}\right|_{V=0} - 0.82\,S} \tag{17}$$

where dI/dV(V=0) is the slope at the inflection point, I_{s1} and I_{s2} are the saturation currents, and S is the slope of the curve in the saturation region. Typically some hysterisis is present, most likely due to probe contamination. The hysterisis does not diminish when the amplitude of the probe voltage is reduced. If the cause of the hysterisis were probe heating, then the opposite would be expected.

To determine the ion density, the Bohm criterion for ion saturation is used. The ion density is then given by[38]

$$n_i = \frac{(0.61)\,I_s}{eA_p}\sqrt{\frac{M_+}{T_e}} \tag{18}$$

where M_+ is the ion mass, I_s is the saturation current, A_p is the surface

area of the probe, and T_e is the electron temperature as found in equation (17). By the quasi-neutrality assumption, the electron density is estimated to be equal to the ion density.

VI. RESULTS

Langmuir probe data was obtained for discharges in both helium and nitrogen. Values required by equations (17) and (18) are obtained from the voltage-current characteristics generated from the Langmuir probes. Electron temperature and ion densities are then calculated and shown in Figs. 7-10.

The electron temperature as a function of pressure obtained for helium and nitrogen discharges is shown in Fig. 7. The discharge power is set to a constant value of 65 watts while the discharge pressure is varied. For low pressure discharges, the electron temperature for helium is larger than that of nitrogen discharges. The increase in electron temperature for low pressures is typical of rf discharges. At low pressures, the electron temperature must increase to sustain a discharge since a decrease in the neutral density lowers the ionization rate. The actual error involved with these measurements is estimated to be sizable because double probes sample only the tail of the electron energy distribution. A high energy tail will therefore lead to an over estimation of the electron temperature.

The electron density as a function of pressure at a constant power of 65 watts in helium and nitrogen is shown in Figs. 8. The error bar shown in the electron density obtained from the Langmuir probe is an estimation of the error in the measurements due to the probable inaccuracy of the electron temperature. Obviously, there are other error components to consider.

Cavity perturbation and the electromagnetic analysis provide measurements of the electron density and collision frequency. To calculate collision frequencies from the Langmuir probe data, equation (6) is used. Assuming the electrons are described by a Maxwellian distribution and using the electron temperature obtained with the floating probe, an effective collision frequency may be calculated by integrating equation (6) over the cross-section for the gas in question. Due to the nature of the cross-section for helium, the collision frequency for helium is predicted[39] to be proportional to the reduced pressure of the discharge.

The collision frequency as a function of pressure in helium and nitrogen is shown in Figs. 9. Values calculated using the Langmuir probe data are compared with those obtained by the electromagnetic analysis and cavity perturbation techniques. The solid line in Fig. 9a shows the collision frequency for helium as predicted by S.C. Brown.[39] Generally the collision frequency increases with pressure. This is due to the fact that as the pressure increases, $\nu(v)$ in equation (6) increases with the neutral density since

$$\nu(v) = N v \sigma(v) \propto \frac{P}{T_g} \tag{19}$$

where $\sigma(v)$ is the momentum transfer cross section, N is the neutral density, P is the discharge pressure, and T_g is the neutral gas temperature. The collision frequencies obtained by the three diagnostics agree with this trend, although the values obtained with the electromagnetic analysis are disappointing. The assumption in the electromagnetic analysis of an isotropic discharge filling the length of the cavity may result in the large

error.

The electron density as a function of power at a constant pressure is shown in Figs. 10. Data is shown for the helium discharges at a fixed discharge pressure of 10 torr, while data for the nitrogen discharges is obtained at 2 torr. One interesting result is that the electron density does not generally increase with the discharge power as may be expected. As noted in similar experiments[24], as the discharge power increases the volume of the discharge also increases, thereby maintaining a constant power density. It is important to realize that with this type of experiment the volume of the discharge varies under different conditions because the discharge is not bound in the axial direction.

The collision frequencies for helium and nitrogen discharges (not shown) did not vary with power due to the constant pressure. Since the power density is roughly constant, the neutral gas temperature in equation (19) also does not change.

The major experimental sources of error are measurements of the discharge power, the frequency shifts, and the discharge volume. More fundamental sources of error are the assumptions inherent to the techniques. To estimate the experimental contribution to the error, solutions of the analyses may be found after varying the experimental input by reasonable amounts. For instance, an error in cavity length measurements of approximately 5% leads to a half order of magnitude difference in the resulting electron densities. However, comparison of the data obtained with the three techniques indicates that despite the assumptions and measurement errors, there is rough agreement between the diagnostics. The classical and 'exact' perturbation analyses yield similar results, even though the electron densities involved are well above

the accepted limit.

The electron temperature measured by the double Langmuir probes actually comes from a sampling of the high energy 'tail' electrons of the discharge. The electron temperature subsequently affects calculations of the ion density from the double probe data. Because the electron temperatures reported here are much higher than those generally found in rf discharges, it is reasonable that the actual electron densities are higher than those calculated from the double probes data.

It should also be noted that while the Langmuir probe obtains the electron density at fixed positions, the electron density obtained by the electromagnetic analysis and 'exact' perturbation analysis is an average over the volume of the discharge. The classical perturbation technique uses an assumed spatial variation of the electron density. However, the other analyses ignore the spatial variations of the conductivity (see equations (7)). Other techniques are available which take this into account,[40] but these complexities have not been implemented into the present diagnostic.

VII. CONCLUSION

Diagnostic techniques are studied and applied to an Asmussen resonant microwave cavity to measure the electron density and collision frequency of resonant cavity discharges. Data is obtained through a range of operating pressures and powers in nitrogen and helium discharges.

The classical perturbation technique first introduced by J.C. Slater is studied. The classical analysis studies the effect the discharge conductance places on the lumped discharge-microwave cavity circuit. By assuming the electromagnetic fields are not affected by the discharge, the microwave

cavity is treated by electronic circuit theory. Theory predicts that this assumption limits the use of the classical analysis to low electron density discharges. However, as shown in this publication, inclusion of the spatial variations of the electron density allow the analysis to be applied to higher densities while incuring errors less than those predicted.

To remove the limitations on the electron density, the discharge is treated from an electromagnetic standpoint. By modeling the discharge as a lossy dielectric, the electromagnetic fields in the presence of a discharge are determined. Boundary conditions governing the fields are then used to produce a characteristic equation. Solutions of the characteristic equation yield the complex conductivity of the discharge as a function of the perturbed resonant quantities of the cavity. Discharge theory then relates the conductivity to the electron density and collision frequency of the discharge. The electromagnetic analysis presented accurately accounts for the spatial attenuation of the electromagnetic fields. In contrast, prior analyses assume that the fields are temporally attenuated.

The corrected electromagnetic fields used in the electromagnetic analysis may also be used in conjunction with perturbation theory. This also eliminates the limitations of the classical perturbation technique. An 'exact' perturbation integral is derived which predicts the shift in the microwave frequency neccesary to compensate for the presence of the discharge.

The use of floating double Langmuir probes provides reasonable data which is consistent in trend with similar types of discharges, such as rf discharges. Disruption of the electromagnetic fields caused by the metallic probe wires is minimal, as shown by measurements of the cavity quality factor with the probe wires present. With the use of a simple sweeping

circuit, the double Langmuir probes provide quick estimates of the electron density, electron temperature, and collision frequency of the resonant cavity discharge. These measurements are then easily compared with results from other diagnostics.

ACKNOWLEDGMENTS

The authors wish to thank Y.Y. Lau for his assistance regarding electromagnetic theory. This research is supported by DOE grant DE-SG07-89ER12891.

APPENDIX

A. Fundamental equation.

The resonant cavity is broken into three radial regions: 1) the discharge, 2) the quartz containment vessel, and 3) the free space extending to the cavity walls. Boundary conditions applied to the electromagnetic fields at the interfaces of the regions may be displayed in matrix form, given by

$$\begin{vmatrix} J_0(k_{\rho 1}a) & -J_0(k_{\rho 2}a) & -Y_0(k_{\rho 2}a) & 0 & 0 \\ 0 & J_0(k_{\rho 2}b) & Y_0(k_{\rho 2}b) & -J_0(k_{\rho 3}b) & -Y_0(k_{\rho 3}b) \\ 0 & 0 & 0 & J_0(k_{\rho 3}c) & Y_0(k_{\rho 3}c) \\ \frac{\varepsilon_1}{k_{\rho 1}}J_1(k_{\rho 1}a) & -\frac{\varepsilon_2}{k_{\rho 2}}J_1(k_{\rho 2}a) & -\frac{\varepsilon_2}{k_{\rho 2}}Y_1(k_{\rho 2}a) & 0 & 0 \\ 0 & \frac{\varepsilon_1}{k_{\rho 2}}J_1(k_{\rho 2}b) & \frac{\varepsilon_2}{k_{\rho 2}}J_1(k_{\rho 2}b) & -\frac{\varepsilon_3}{k_{\rho 3}}J_1(k_{\rho 3}b) & -\frac{\varepsilon_3}{k_{\rho 3}}Y_1(k_{\rho 3}b) \end{vmatrix} \begin{vmatrix} A_1 \\ A_2 \\ B_2 \\ A_3 \\ B_3 \end{vmatrix} = \begin{vmatrix} 0 \\ 0 \\ 0 \\ 0 \\ 0 \end{vmatrix} \quad (A.1)$$

Setting the determinant of the first matrix equal to zero leads to the characteristic equation, given by

$$\frac{k_{\rho 2}\varepsilon_3 c_1}{k_{\rho 3}\varepsilon_2 c_2} = \frac{c_3 Y_1(k_{\rho 2}b) + c_4 J_1(k_{\rho 2}b)}{c_3 Y_0(k_{\rho 2}b) + c_4 J_0(k_{\rho 2}b)} \tag{A.2}$$

where

$$c_1 = J_1(k_{\rho 3}b) - J_0(k_{\rho 3}c)\frac{Y_1(k_{\rho 3}b)}{Y_0(k_{\rho 3}c)} \tag{A.3a}$$

$$c_2 = J_0(k_{\rho 3}b) - J_0(k_{\rho 3}c)\frac{Y_0(k_{\rho 3}b)}{Y_0(k_{\rho 3}c)} \tag{A.3b}$$

$$c_3 = J_1(k_{\rho 1}a)\frac{J_0(k_{\rho 2}a)}{J_0(k_{\rho 1}a)}\frac{\varepsilon_1}{k_{\rho 1}} - J_1(k_{\rho 2}a)\frac{\varepsilon_2}{k_{\rho 2}} \tag{A.3c}$$

$$c_4 = Y_1(k_{\rho 2}a)\frac{\varepsilon_2}{k_{\rho 2}} - Y_0(k_{\rho 2}a)\frac{J_1(k_{\rho 1}a)}{J_0(k_{\rho 1}a)}\frac{\varepsilon_1}{k_{\rho 1}} \tag{A.3d}$$

ε_1 is found using equation (2), $\varepsilon_2 = 3.78\,\varepsilon_0$ (dielectric of quartz), $\varepsilon_3 = \varepsilon_0$, and the J's and Y's are Bessel's functions of the first and second kind. The quantities a, b, and c are the radii of the three coaxial regions. The characteristic equation provides the conductivity of the first region as a function of the cavity length and attenuation of the electromagnetic fields.

The shifted cavity length as a function of the electron density predicted by the characteristic equation is shown in Fig. 11. It is interesting to note that the characteristic equation correctly predicts a new resonant cavity length, shorter than that of an unloaded cavity, when the cavity is loaded with the quartz vacuum vessel. The dielectric permittivity

of the quartz tube is higher than that of free space causing an downward shift in cavity length, while the permittivity of a discharge is lower than that of free space causing an upward shift in cavity length.

Solutions of the characteristic equation show that as the attenuation constant approaches zero, the real portion of the conductivity also approaches zero. Because the dissipated power is proportional to the real component of the conductivity, the spatial attenuation is a direct result of the presence of the lossy material and results in power being absorbed by the lossy material.

B. Electromagnetic fields.

By introducing the axial regions to the fields shown in equations (3), the electromagnetic waves in region X ($0<z<L_{ant}$) remain the same as equations (3), while in region Y ($L_{ant}<z<L$) they are given by

$$E_{\rho i}(\rho,\theta,z,t) =$$

$$-\frac{jk_z}{k_{\rho i}}\exp\{j\omega t\}\sinh\{jk_z(z-L)\}\frac{\sinh\{jk_z(L_{ant})\}}{\sinh\{jk_z(L_{ant}-L)\}}\left[A_iJ_1(k_{\rho i}\rho)+B_iY_1(k_{\rho i}\rho)\right] \quad \text{(A.4a)}$$

$$E_{zi}(\rho,\theta,z,t) =$$

$$\exp\{j\omega t\}\cosh\{jk_z(z-L)\}\frac{\sinh\{jk_zL_{ant}\}}{\sinh\{jk_z(L_{ant}-L)\}}\left[A_iJ_0(k_{\rho i}\rho)+B_iY_0(k_{\rho i}\rho)\right] \quad \text{(A.4b)}$$

$$B_{\theta i}(\rho,\theta,z,t) =$$

$$\frac{j\omega\mu_0\varepsilon_i}{k_{\rho i}}\exp\{j\omega t\}\cosh\{jk_z(z-L)\}\frac{\sinh\{jk_zL_{ant}\}}{\sinh\{jk_z(L_{ant}-L)\}}\left[A_iJ_1(k_{\rho i}\rho)+B_iY_1(k_{\rho i}\rho)\right] \quad \text{(A.4c)}$$

$$E_{\theta i}(\rho,\theta,z,t) = 0 \quad \text{(A.4d)}$$

$$B_{\rho i}(\rho,\theta,z,t)=0 \tag{A.4e}$$

$$B_{zi}(\rho,\theta,z,t)=0 \tag{A.4f}$$

Shown in Fig. 3 is the standing wave predicted by these fields, as well as a set of electric field probe data showing the attenuation present.

C. Cavity perturbation.

Assuming time harmonic electromagnetic waves, Maxwell's equations may be written as

$$\overline{\nabla}\times\overline{E}=-j\omega\overline{B} \tag{A.5a}$$

$$\overline{\nabla}\times\overline{B}=\mu_0(\sigma+j\varepsilon_0\omega)\overline{E} \tag{A.5b}$$

Assume that the presence of the discharge results in a microwave frequency shift and a complex frequency. The electromagnetic fields are then simply

$$E_{\rho i}(\rho,\theta,z,t)=\frac{k_z}{k_{\rho i}}\exp\{j\omega t\}\sin\{k_z z\}\left[A_i J_1(k_{\rho i}\rho)+B_i Y_1(k_{\rho i}\rho)\right] \tag{A.6a}$$

$$E_{zi}(\rho,\theta,z,t)=\exp\{j\omega t\}\cos\{k_z z\}\left[A_i J_0(k_{\rho i}\rho)+B_i Y_0(k_{\rho i}\rho)\right] \tag{A.6b}$$

$$B_{\theta i}(\rho,\theta,z,t)=j\frac{\omega\mu_0\varepsilon_i}{k_{\rho i}}\exp\{j\omega t\}\cos\{k_z z\}\left[A_i J_1(k_{\rho i}\rho)+B_i Y_1(k_{\rho i}\rho)\right] \tag{A.6c}$$

where k_z and $k_{\rho i}$ are the same as in equations (4), except that now α is zero

while the frequency ω is complex.

Maxwell's equations must hold whether or not there is a discharge present. If we take the dot product of the electric field with equation (A.5b) and integrate over the volume of region i, we obtain

$$\int_{\text{region } i} \bar{E} \bullet \left(\bar{\nabla} \times \bar{B}\right) dV = \int_{\text{region } i} j\mu_0 \varepsilon_i \omega \bar{E} \bullet \bar{E} dV \qquad \text{(A.7)}$$

The first integral may be broken into two components, $\nabla \bullet (B \times E) + B \bullet (\nabla \times E)$. The second component is replaced using equation (A.5a). The first component is solved using the divergence theorem, and becomes a surface integral over the surface of region i. However, at the interface of two regions, this integral will cancel, since the normal vector is in opposite directions while the fields are continuous at the interface. Therefore, if we sum equation (A.7) over the three regions, the only surface integral left will be the one over the surface of the cavity walls. However, this surface integral is approximately zero due to the high conductivity of the cavity walls. What is left is then

$$\int_{\text{cavity}} \left\{ \bar{B} \bullet \bar{B} + \mu_0 \varepsilon \bar{E} \bullet \bar{E} \right\} dV = 0 \qquad \text{(A.8)}$$

Here, the dot product represents the square of complex quantities and is not necessarily a positive definite quantity, such as a quantity dotted with its conjugate. Inspection of equations (A.6) shows that the square of the magnetic field is negative, while the square of the electric fields is positive.

While equation (A.8) may not look like a typical perturbation equation, the equation must hold at any frequency. The shift in the

resonant frequency is a result of the presence of the discharge and the quartz vacuum vessel. In other words, for a given complex conductivity, the microwave frequency becomes complex and shifts such that equation (A.8) still holds.

REFERENCES

[1]J. Asmussen, J. Vac. Sci. Technol. A 7(3), 883 (1989).

[2]T. Hatakeyama, F. Kannari, and M. Obara, Appl. Phys. Lett. 59(4). 387 (1991).

[3]H. Kumagai and K. Toyoda, Appl. Phys. Lett. 59(22). 2811 (1991).

[4]W. McColl, M. Passow, and M.L. Brake, Rev. Sci. Instrum. 63(2), 1792 (1992).

[5]J.C. Slater, Rev. Modern Phys. 18, 441 (1946).

[6]S.C. Brown, et al., Tech. Rept. No. 66, Research Laboratory of Electronics, M.I.T. (1948).

[7]D.J. Rose, D.E. Kerr, M.A. Biondi, E. Everhart, and S.C. Brown, Tech. Rept. No. 140, Research Laboratory of Electronics, M.I.T. (1949).

[8]M.A. Biondi, Rev. Sci. Instrum. 22(7), 500 (1951).

[9]S.C. Brown, and D.J. Rose, J. Appl. Phys. 23(7), 711 (1952).

[10]D.J. Rose, and S.C. Brown, J. Appl. Phys. 23(7), 718 (1952).

[11]D.J. Rose, and S.C. Brown, J. Appl. Phys. 23(9), 1028 (1952).

[12]L. Gould, and S.C. Brown, J. Appl. Phys. 24(8), 1053 (1953).

[13]K.B. Persson, Phys. Rev. 106(2), 191 (1957).

[14]S.J. Buchsbaum, and S.C. Brown, Phys. Rev. 106(2), 196 (1957).

[15]M.A.W. Vlachos, and H.C.S. Hsuan, J. Appl. Phys. 39(11), 5009 (1968).

[16]C.J. Burkley, and M.C. Sexton, J. Appl. Phys. 39(11), 5013 (1968).

[17]S.C. Brown, Proc. 2nd U.N. Intern. Conf. Peaceful Uses of Atomic Energy 32, 394 (1958).

[18]S.J. Buchsbaum, L. Mower, and S.C. Brown, Phys. Fluids 3(5), 806 (1960).

[19]B. Agdur and B. Enander, J. Appl. Phys. 33(2), 575 (1962).

[20]J.L. Shohet, and C. Moskowitz, J. Appl. Phys. 36(5), 1756 (1965).

[21]D.E. Kerr, S.C. Brown, and Kern, Phys. Rev. 71, 480 (1949).

[22]P. Rosen, J. Appl. Phys. 20, 868 (1949).

[23]E.B. Manring, Ph.D. thesis, Michigan State University, 1992.

[24]W. McColl, M.S. thesis, University of Michigan, 1990.

[25]M.L. Passow, M.L. Brake, P. Lopez, W. McColl, and T. Repetti, IEEE Trans. Plasma Sci. 19, 219 (1991).

[26]J.Rogers, Ph.D. thesis, Michigan State University, 1982.

[27]G. King, F.C. Sze, P. Mak, T.A. Grotjohn, and J. Asmussen, J. Vac. Sci. Technol. A 10(4), 1265 (1992).

[28]J. Hopwood, and J. Asmussen, Appl. Phys. Lett. 58(22), 2473 (1991).

[29]W. McColl, C. Brooks, and M.L. Brake, to be published, J. Vac. Sci. Technol. A (August 1993).

[30]R.F. Harrington, Time-Harmonic Electromagnetic Fields, (McGraw-Hill, New York, 1961).

[31]B.E. Cherrington, Gaseous Electronics and Gas Lasers, (Pergamon Press, New York, 1979).

[32]R.F. Whitmer, and G.F. Herrmann, Phys. Fluids 9(4), 768 (1966).

[33]J. Asmussen, R. Mallavarpu, J. Hamann, and H. Park, Proc.

IEEE 62, 109 (1974).

[34]R. Mallavarpu, J. Asmussen, and M.C. Hawley, IEEE Trans. Plasma Sci. PS 6, 341 (1978).

[35]J.D. Swift, and M.J.R. Schwar, Electrical Probes for Plasma Diagnostics, (Iliffe Books, London, 1969).

[36]E.O. Johnson, and L. Malter, Phys. Rev. 80(1), 58 (1950).

[37]T. Dote, Jpn. J. Appl. Phys 7, 964 (1968).

[38]N. Hershkowitz, in Plasma Diagnostics Vol. I, edited by O. Auciello, and D.L. Flamm, (Academic Press, San Diego, 1989).

[39]S.C. Brown, Introduction to Electrical Discharges in Gases, (John Wiley&Sons, New York, 1966).

[40]S. Offermanns, J. Appl. Phys. 67(1), 115 (1990).

FIGURE CAPTIONS

Fig. 1. The various regions utilized by the electromagnetic analysis. The basis of the analysis is that the electromagnetic fields are spatially attenuated as they move away from the microwave coupling antenna.

Fig. 2. An outline of the steps used by the electromagnetic analysis.

Fig. 3. Samples of the radial electric field (●), as well as the standing wave predicted ι_y the electromagnetic analysis (solid line). The attenuation of the standing wave is a result power being absorbed by the discharge. The null position in the middle of the cavity is utilized to insert double Langmuir probe wires into the discharge.

Fig. 4. Samples of the light emitted by a discharge as a function of position along the cavity axis (●). The discharge is bounded axially by the positions L_{start} and L_{stop}, and in general follows $\cos^2(2\pi z/L)$ (solid line).

Fig. 5. The shift in the microwave frequency for various electron densities for a TM_{012} mode. The resonant microwave frequency is 2.45 GHz. The solid line corresponds to solutions from the 'exact' technique. The dashed line is from the classical perturbation technique for a plasma which fills the length of the cavity, while the dashed line with circles corresponds to a discharge filling half the cavity. The exact technique accounts for the presence of the quartz tube, while the classical technique does not.

Fig. 6. A schematic of the Asmussen resonant microwave cavity used in

the experiment. Variations in the cavity length are necessary to account for the perturbation caused by the discharge.

Fig. 7. The electron temperature as a function of pressure obtained for helium (●) and nitrogen (O) discharges.

Fig. 8a. The electron density as a function of pressure at a constant power of 65 watts obtained for helium determined by the double Langmuir probe (▲), electromagnetic analysis (●), classical perturbation technique (■), and 'exact' perturbation technique (Δ).

Fig. 8b. The electron density as a function of pressure at a constant power of 65 watts obtained for nitrogen determined by the double Langmuir probe (▲), electromagnetic analysis (●), classical perturbation technique (■), and 'exact' perturbation technique (Δ).

Fig. 9a. The collision frequency as a function of pressure at a constant power of 65 watts obtained for helium determined by the double Langmuir probe (▲), electromagnetic analysis (●), classical perturbation technique (■), and 'exact' perturbation technique (Δ). The solid line shows values predicted by S.C. Brown.[39]

Fig. 9b. The collision frequency as a function of pressure at a constant power of 65 watts obtained for nitrogen determined by the double Langmuir probe (▲), electromagnetic analysis (●), classical perturbation technique (■), and 'exact' perturbation technique (Δ).

Fig. 10a. The electron density as a function of power at a constant pressure of 10 torr obtained for helium determined by the double Langmuir probe (▲), electromagnetic analysis (●), classical perturbation technique (■), and 'exact' perturbation technique (Δ).

Fig. 10b. The electron density as a function of power at a constant pressure of 2 torr obtained for nitrogen determined by the double Langmuir probe (▲), electromagnetic analysis (●), classical perturbation technique (■), and 'exact' perturbation technique (Δ).

Fig. 11. The shifted cavity length for various electron densities predicted by the electromagnetic analysis at two collision frequencies. The resonant cavity length is 14.4 cm.

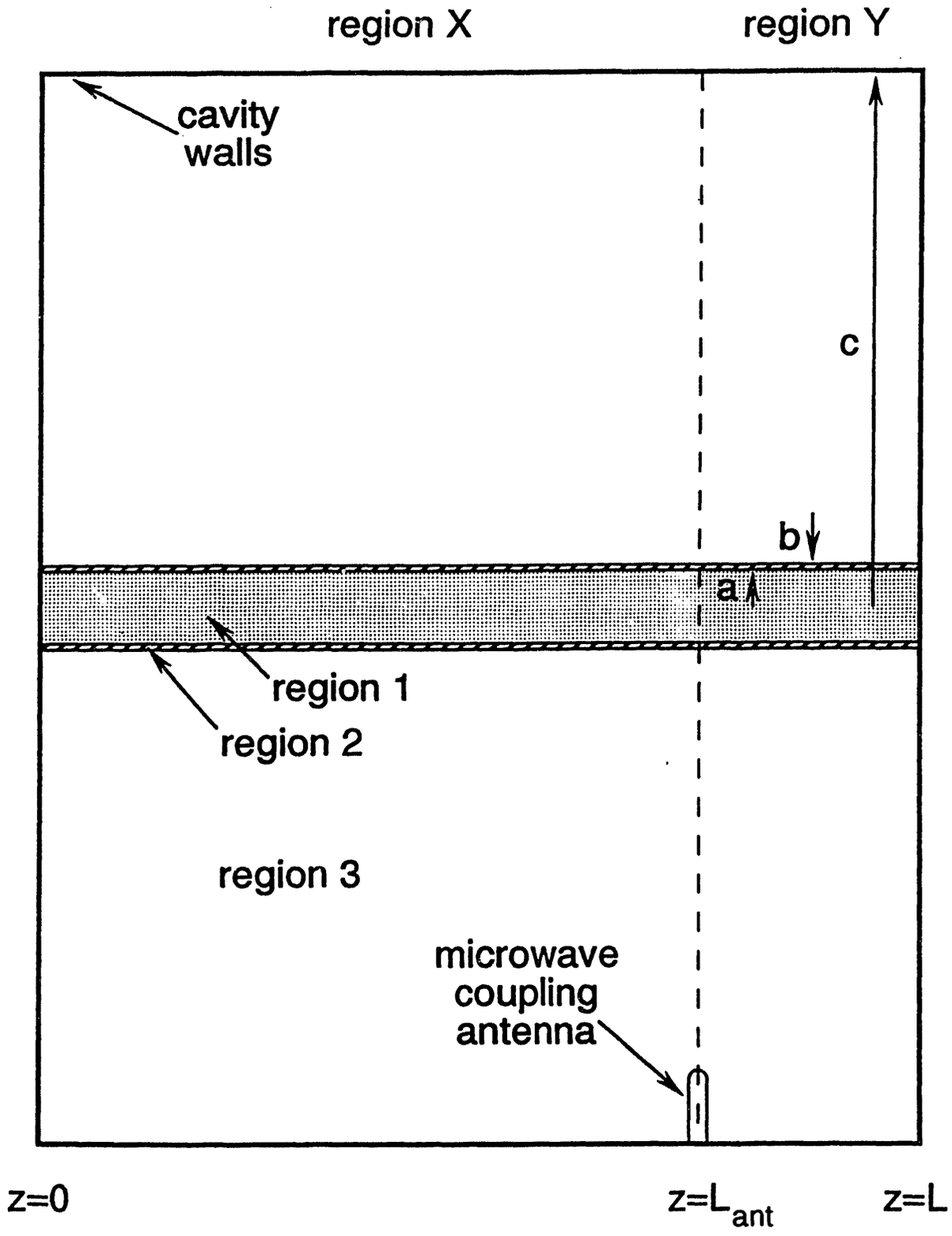
region X
region Y
cavity
walls
c
b
a
region 1
region 2
region 3
microwave
coupling
antenna
z=0
z=L_ant
z=L

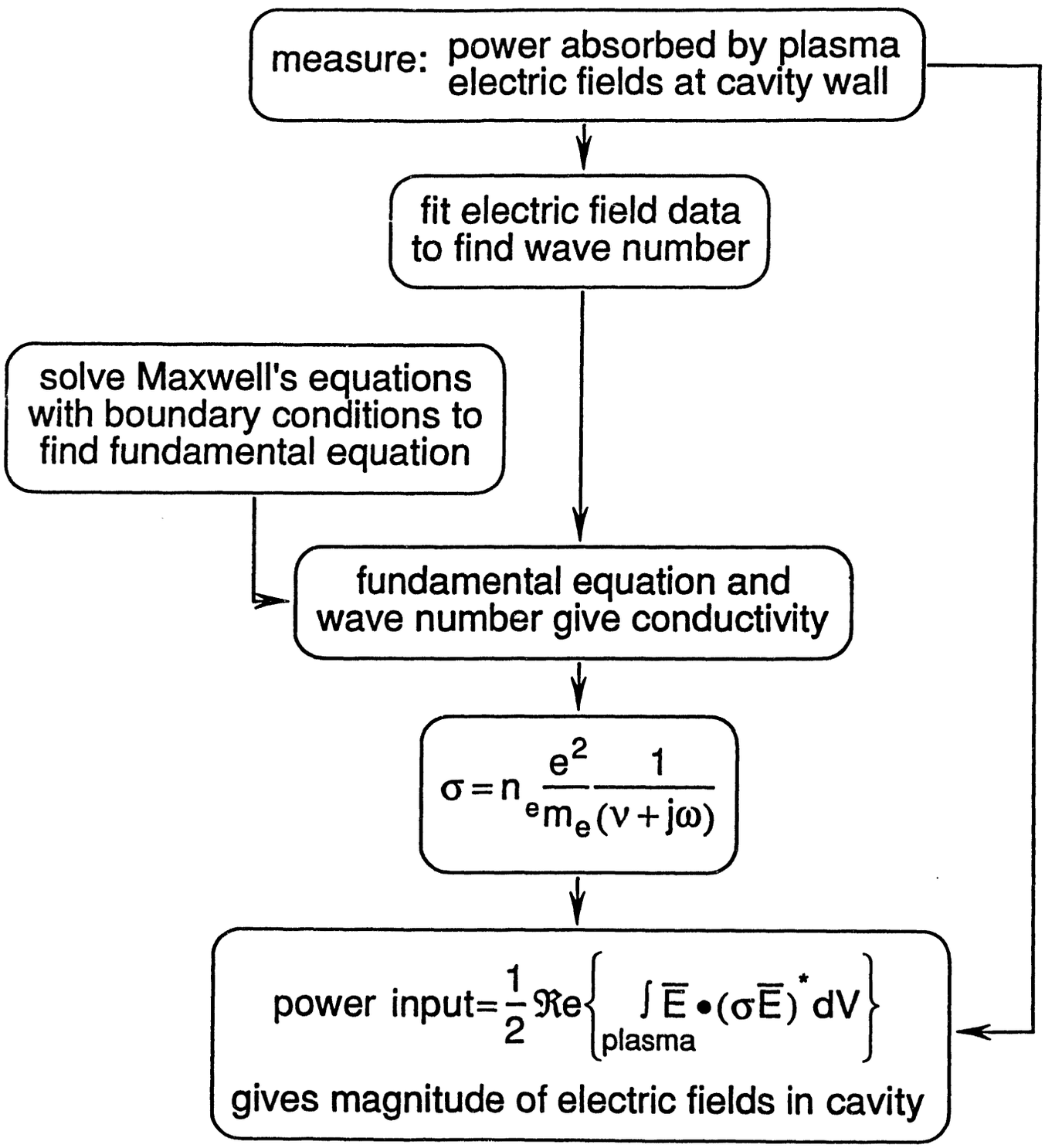
measure: power absorbed by plasma electric fields at cavity wall
fit electric field data to find wave number
solve Maxwell's equations with boundary conditions to find fundamental equation
fundamental equation and wave number give conductivity
$\sigma = n_e \frac{e^2}{m_e} \frac{1}{(\nu + j\omega)}$
power input $= \frac{1}{2} \Re e \left\{ \int_{plasma} \bar{E} \bullet (\sigma \bar{E})^* dV \right\}$
gives magnitude of electric fields in cavity

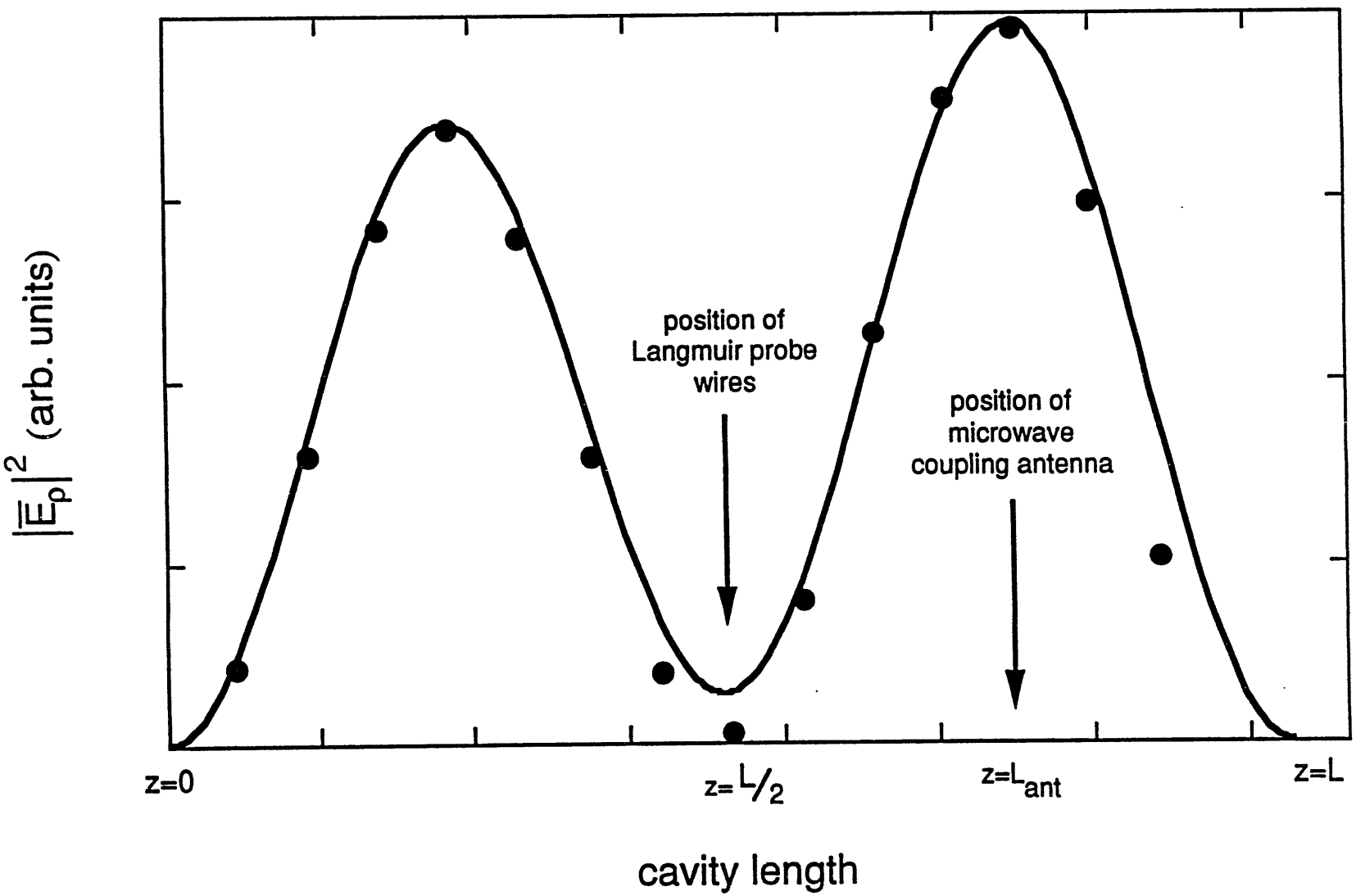
$|\bar{E}_p|^2$ (arb. units)
position of
Langmuir probe
wires
position of
microwave
coupling antenna
z=0
z=L/2
z=L_ant
z=L
cavity length

Fig 3

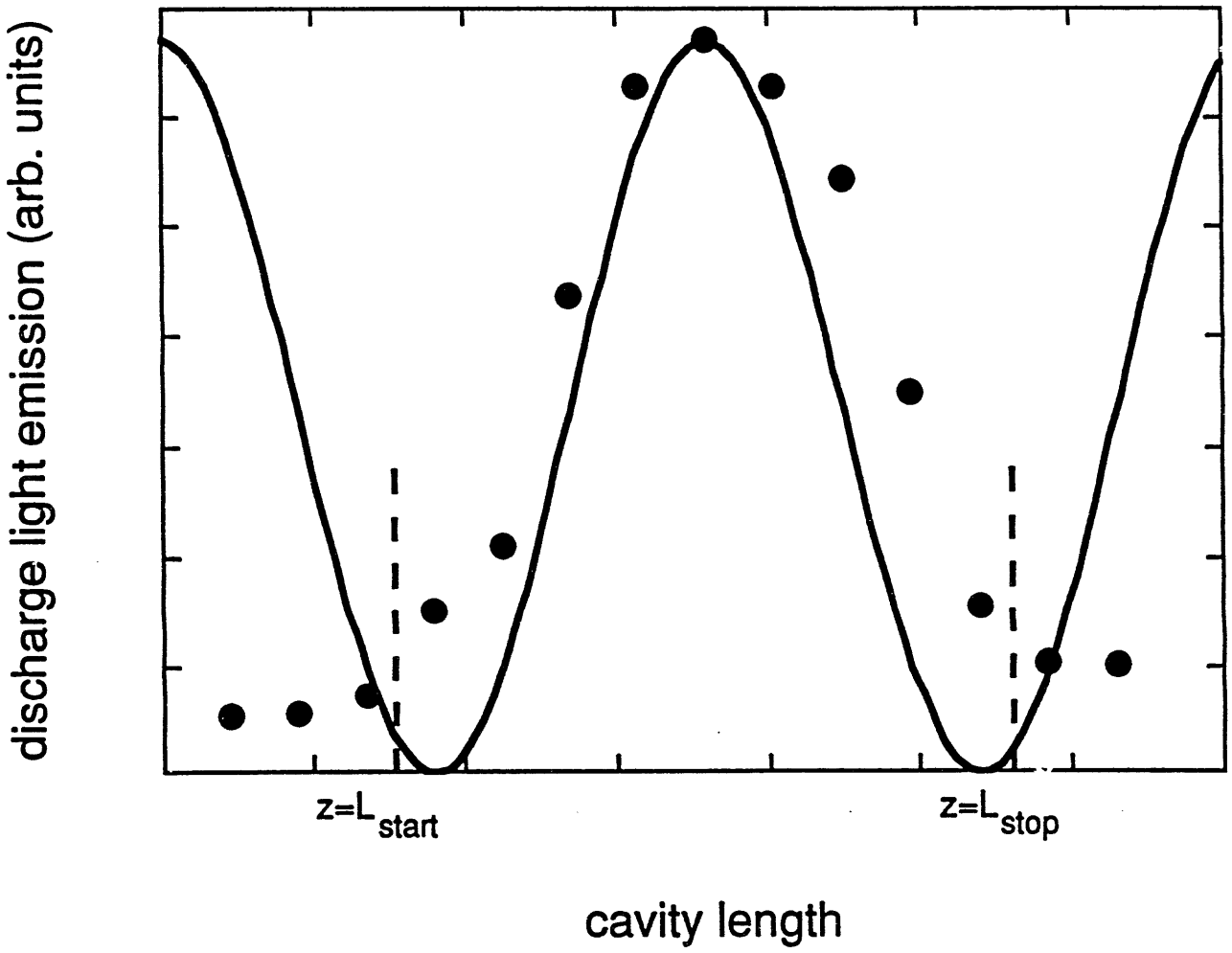
discharge light emission (arb. units)
z=L start
z=L stop
cavity length

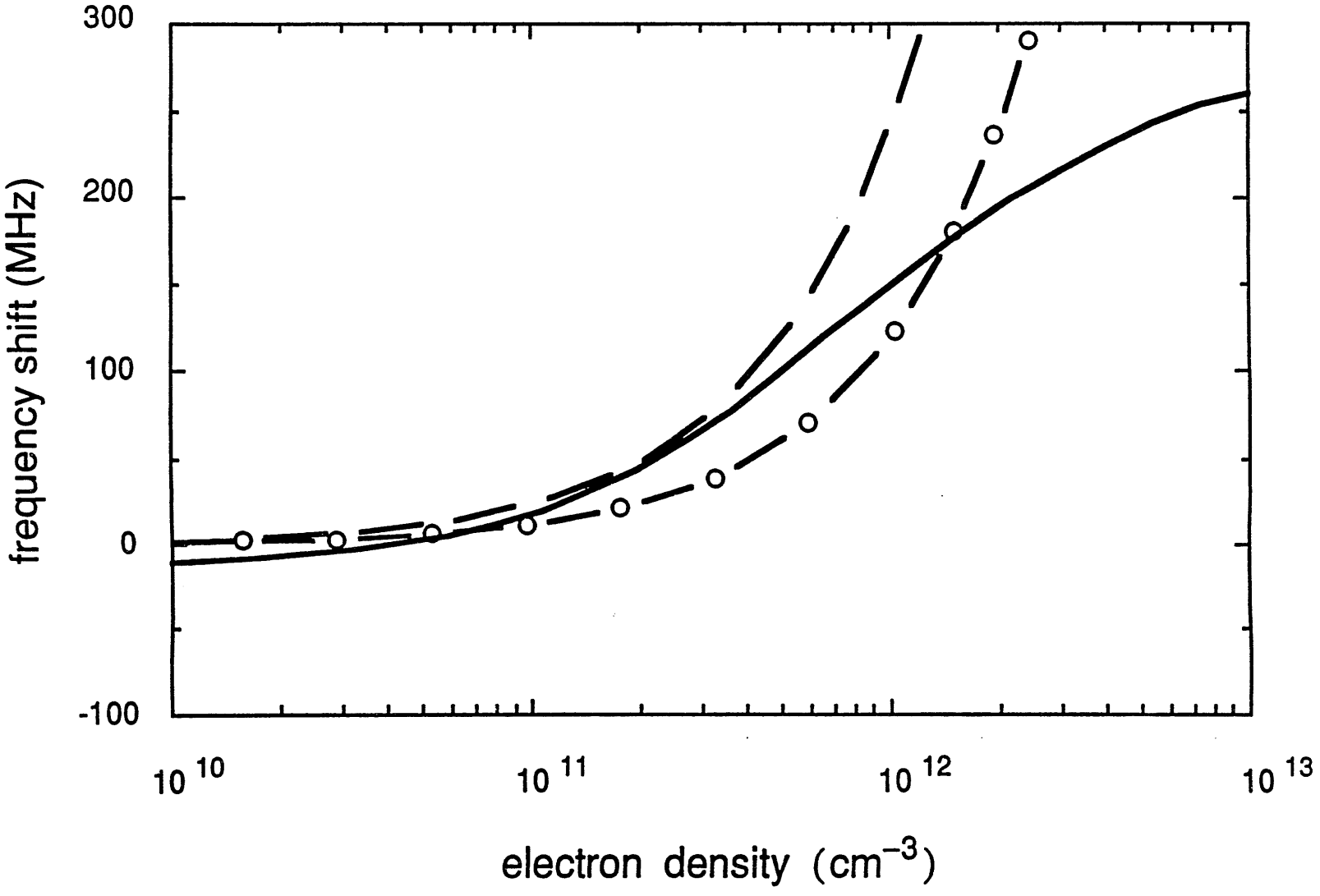
300
200
100
0
-100
frequency shift (MHz)
10 10
10 11
10 12
10 13
electron density (cm−3)

Fig 5

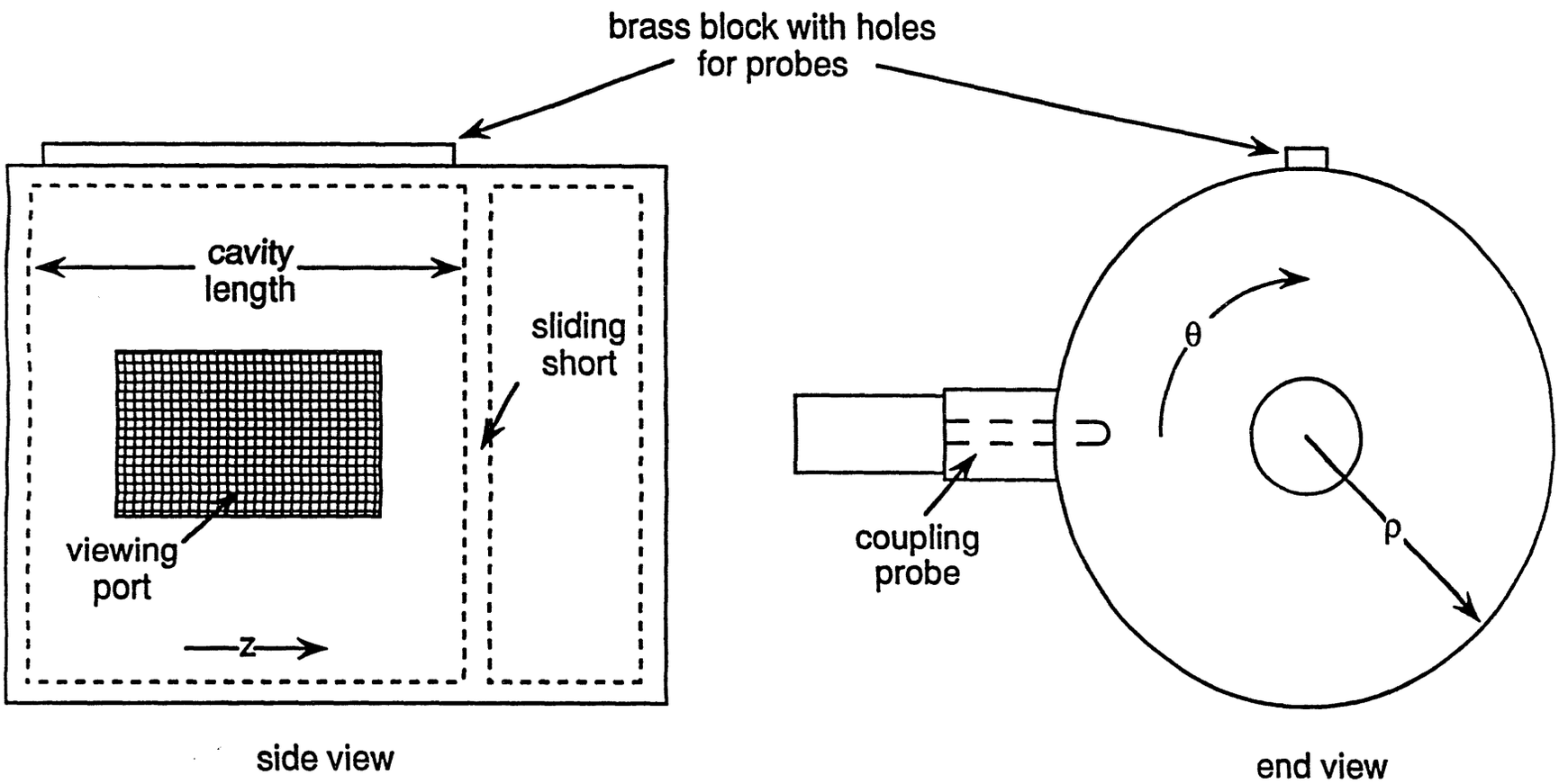
brass block with holes
for probes
cavity
length
sliding
short
viewing
port
z
coupling
probe
θ
ρ
side view
end view

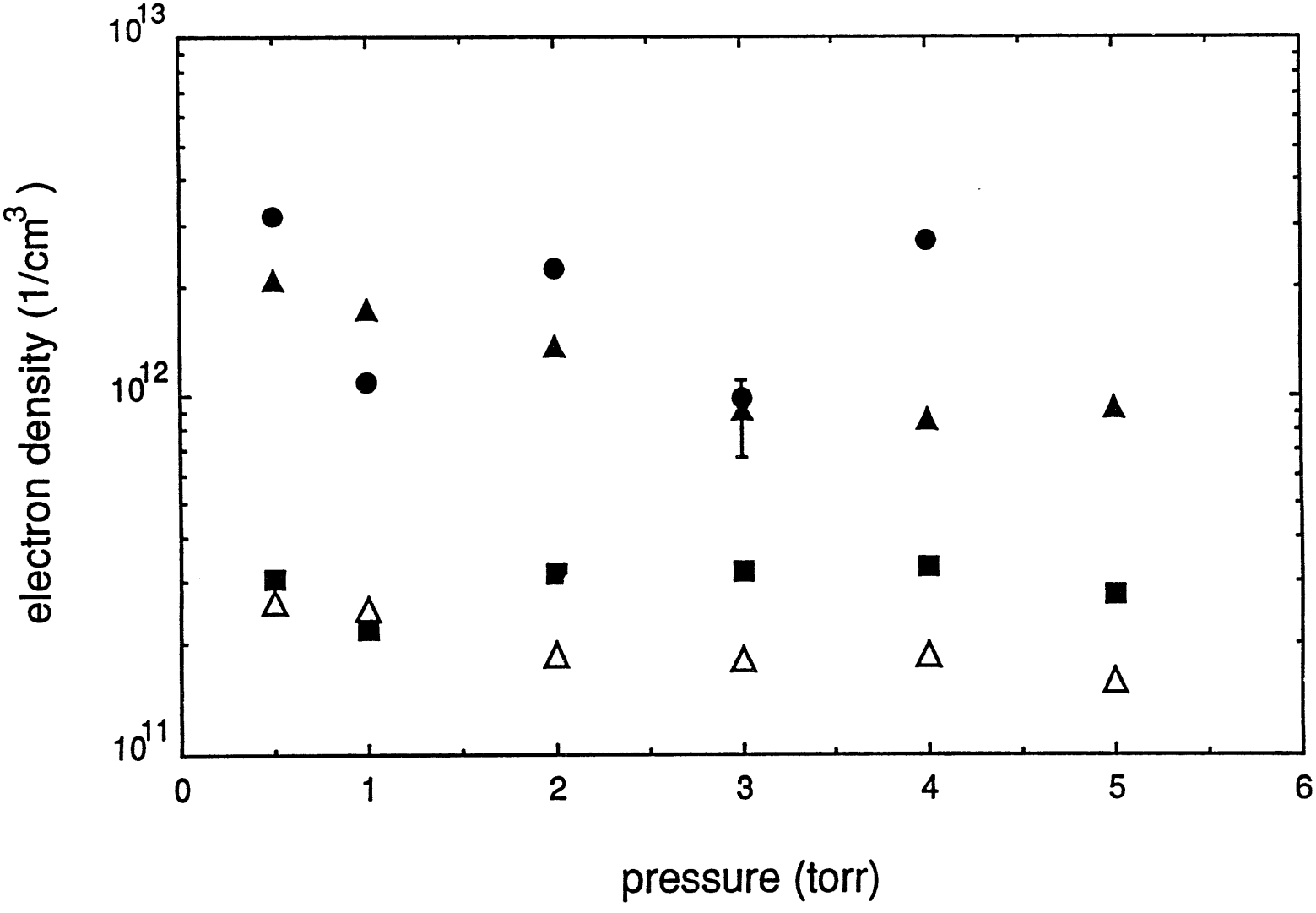
10^{13}
10^{12}
10^{11}
electron density ($1/cm^3$)
0
1
2
3
4
5
6
pressure (torr)

Fig 9a

pressure (torr)
0
1
2
3
4
5
6
collision frequency (1/sec)
10^9
10^{10}
10^{11}

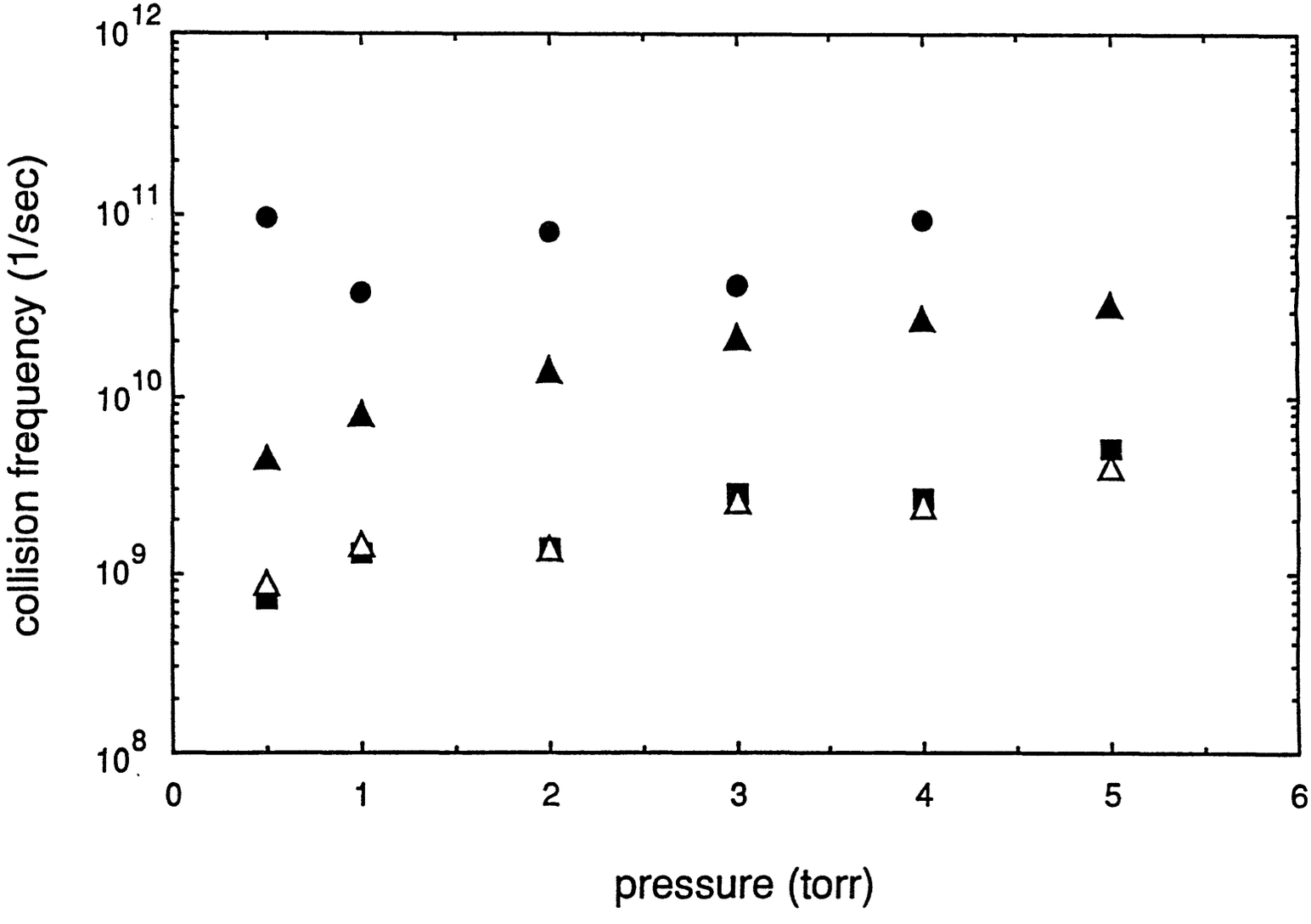
collision frequency (1/sec)
10^{12}
10^{11}
10^{10}
10^{9}
10^{8}
0
1
2
3
4
5
6
pressure (torr)

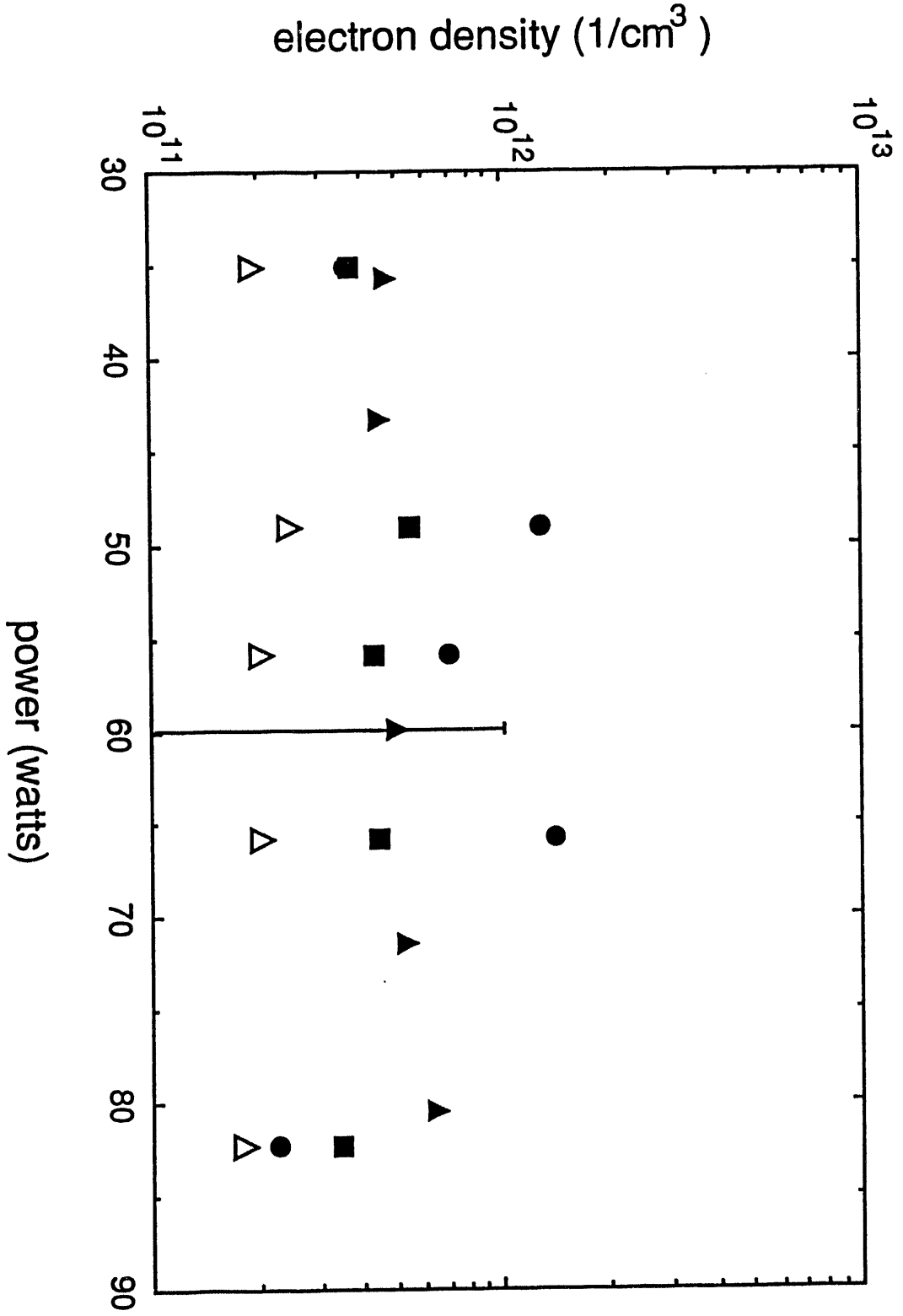
electron density (1/cm^3)
10^{11}
10^{12}
10^{13}
power (watts)
30
40
50
60
70
80
90

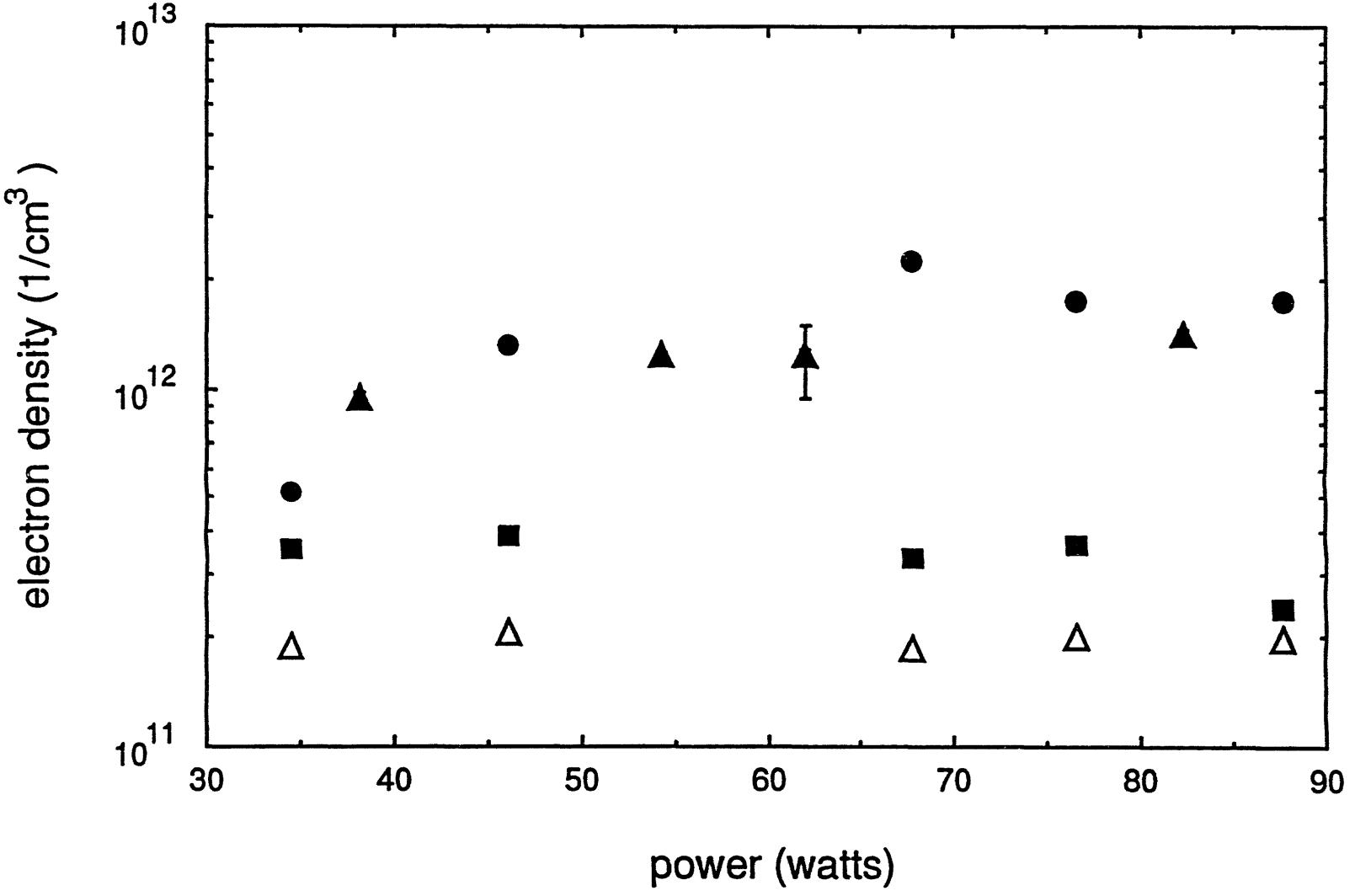
10^{13}
10^{12}
10^{11}
electron density (1/cm^3)
30
40
50
60
70
80
90
power (watts)

Fig 10b

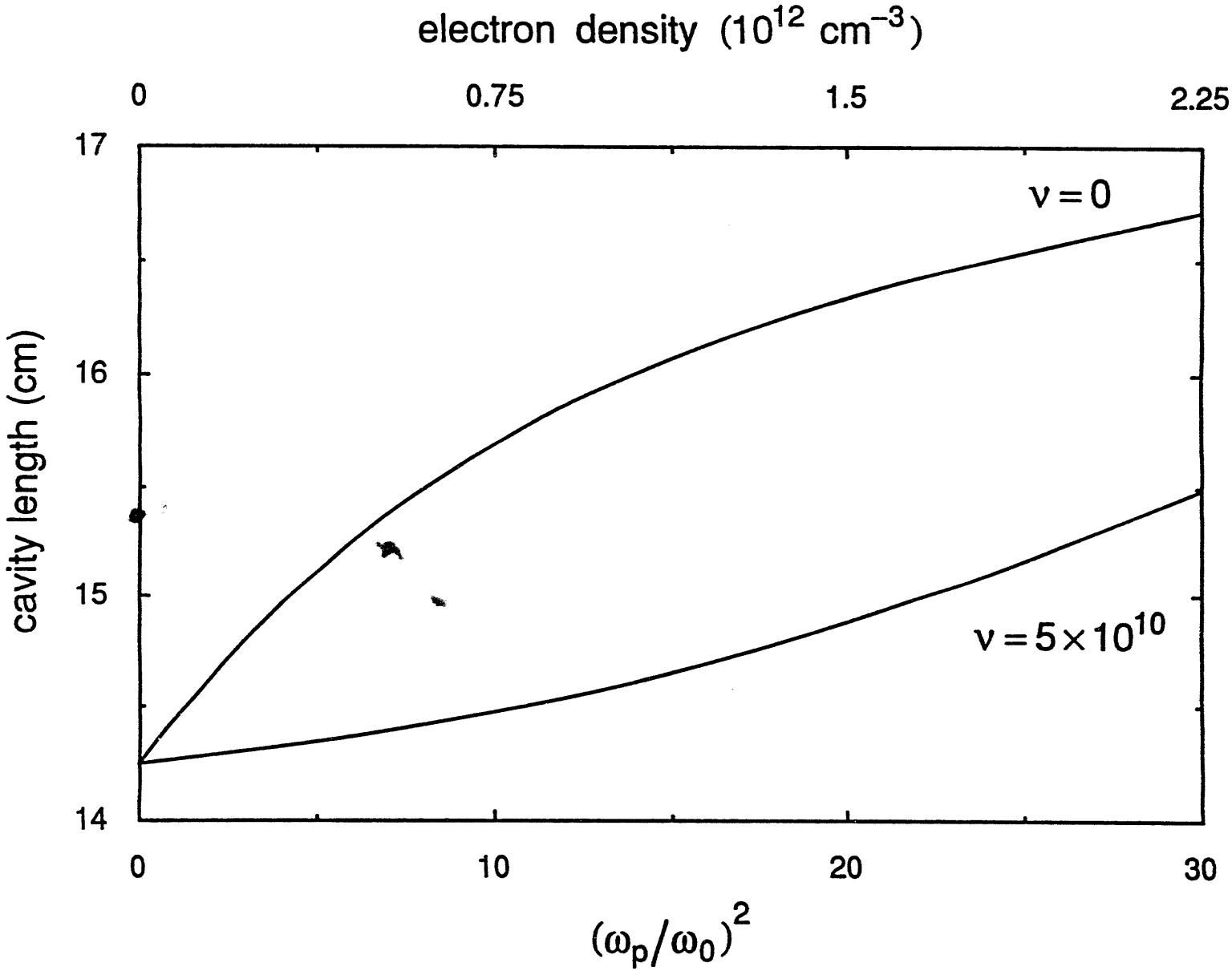
electron density (10^{12} cm^{-3})
0
0.75
1.5
2.25
17
16
15
14
cavity length (cm)
ν = 0
ν = 5×10^{10}
0
10
20
30
$(\omega_p/\omega_0)^2$

IV. D Scaling of Innovative Lasers for large-scale Uranium isotope separation

During the third year of this research program, we will investigate the scaling of the optimal microwave and electron beam - pumped copper vapor laser to production - scale uranium atomic vapor laser isotope separation (AVLIS). Scaling issues which need to be addressed in assessing the utility of microwave and electron beam pumped copper vapor lasers to AVLIS include:

1) Maximum efficiency in conversion of microwave and electron beam energy to laser optical energy,

2) Recirculating power in production scale, repetitively pulsed microwave and electron beam excitation,

3) Heat loading effects on the interior of the laser head, and

4) Maximum volume and output optical energy of individual microwave and electron beam pumped copper vapor lasers.

Based on these studies, a design will be developed for both a microwave and an electron beam pumped copper vapor laser system for a production - scale uranium atomic vapor laser isotope separation facility.

IV. E References

1. B. E. Warner, "An Overview of Copper-Laser Development for Isotope Separation", in **New Developments and Applications in Gas Lasers,** ed. L. R. Carlson, Vol. 737, p. 2, Proceedings of SPIE. 1987.

2. M. J. Kushner and B. E. Warner, "Large-Bore Copper Vapor Lasers: Kinetics and Scaling Issue," J. Appl. Phys., 54, 2920, 1983.

3. R. G. Bosisio, C. F. Weissfloch and M. R. Wertheimer, "The large volume microwave plasma generator", J. Micro. Power, 7, 628, 1972.

4. A. Mendelsohn, R. Normandin, S. Harris and J. Young, "A Microwave Pumped XeCl Laser", Appl. Phys. Letts., 38, 603, 1981.

5. C. Christenson and R. Waynant, "200 MHz Electrodeless discharge excitation of an XeF Laser", Appl. Phys. Lett., 41, 794, 1982.

6. J. Young, S. Harris, P. Wisoff and A. Mendelsohn, "Microwave Excitation of Excimer Lasers", Laser Focus, p. 63, April 1983.

7. C. Christensen and W. Waynant, "High Efficiency Microwave Discharge XeCl Laser", Appl. Phys. Letts., 46, 320, 1985.

8. A. Didenko, V. Petrov, V. Slin'ko, A. Sulakshin, and S. Sulakshin, "Excimer laser pumped by an intense relativistic microwave source", Sov. Tech. Phys. Lett. 12(10), 515, 1986.

9. C. Gordon, B. Feldman, and C. Christensen, "Microwave - discharge excitation of an ArXe laser", Optics Letts., 13, 114, 1988.

10. C. Moutoulas, M. Moisan, L. Bertrand, J. Hubert, J. Lachambre, and A. Ricard, "A high-frequency surface wave pumped He-Ne laser", Appl. Phys. Lett., 46, 323, 1985

11. J. Marec, University of Paris-Sud, private communication

12. Ch. K. Rhodes, ed., Excimer Lasers, Springer Verlag, 1984

13. George Bekefi, Principles of Laser Plasmas, Wiley Interscience, 1976.

14. B. L. Borovich, V. V. Buchanov, and E. I. Molodykh, "Numerical modeling of an electron-beam pumped copper vapor laser", Sov. J. Quantum Electron. 14, 680, 1984.

15. R. Mallavarpu, J. Asmussen and M. C. Hawley, "Behavior of a microwave cavity discharge over a wide range of pressures and flow rates", IEEE Trans. on Plasma Sci., PS-6, 341, 1978.

16. J. Rogers and J. Asmussen, "Standing waves along a microwave generated surface wave plasma", IEEE Trans. on Plasma Sci. PS-10, 11, 1982.

17. S. Whitehair, J. Asmussen and S. Nakanishi, "Microwave electrothermal thruster performance in helium", J. Propulsion and Power, 3, 136, 1987

18. J. Asmussen, R. Mallavarpu, J. Hamann, and H. Park, "The Design of a Microwave Plasma Cavity", Proc. IEEE, 62, 109, 1974.

19. Will McColl, "Measurements of a Copper Chloride Microwave Discharge", M.S. Thesis, University of Michigan, 1990

V. Experience and Qualifications of the Applicants

The project director, Mary L. Brake has been active in the area of microwave and electron beam produced discharges for the past nine years. In the fall of 1984 she became an Assistant Professor of Nuclear Engineering, and since that time has worked on the emission spectroscopy and chemical kinetics of electron beam interactions with gases, as well as microwave excited plasmas. She has recently been promoted to Associate Professor. In 1983 she worked on laser guided discharges as a post doctoral fellow at the University of Michigan. Dr. Brake earned her Ph.D. degree in 1983 from Michigan State University where she investigated the application of microwave plasmas to novel forms of space-craft propulsion. She has published 21 refereed journal articles and has presented 36 conference papers.

Ronald M. Gilgenbach, a co-principal investigator, is a recognized authority concerning the interaction of intense electron beams,high power microwaves, and lasers with plasmas and gases. He founded the Intense Energy Beam Interaction Laboratory in 1980, when he assumed a faculty position in the Nuclear Engineering Department at the University of Michigan. From 1978 through 1980 his research at the Naval Research Laboratory and Oak Ridge National Laboratory resulted in the first definitive experiment in which high power microwaves from an electron beam gyrotron were used to heat a tokamak plasma. Dr. Gilgenbach earned his Ph.D. degree in 1978 from Columbia University, where he investigated high power microwave generation from intense e-beams. He received his B.S. (1972) and M.S. (1973) from the University of Wisconsin, where he performed experiments on microwave heated plasmas. He has published about 50 refereed journal articles and presented over 80 conference papers.

VI. Institutional Resources

A. Experimental Facilities

The following is a list of the Major Experimental Facilities:

Electron Beam Accelerators

1) Michigan Electron Long Beam Accelerator (MELBA):

   - 0.5 to - 1 MV, 1 - 60 kA, 0.3 - 4 μs electron beam parameters,

2) Febetron electron beam generator:

   - 0.4 to - 0.5 MV, 1 to 1.4 kA, 0.3 - 0.4 μs electron beam parameters,

Microwave Experimental Equipment

1) Microwave Resonant Cavity

2) Pulsed microwave power source -0 to 4.5 kW, 0.3 μs to 50 ms pulse width, 20 to 25,000 Hz

High Power Lasers

1) Excimer Laser (Lumonics TE 292-K)

   1.5 J @ 249 nm on KrF in a 25 ns pulse

2) CO_2 Laser (Lumonics 601A)

   15J (50 J) in 100 ns (2μs) pulse @ 10.6 μm

3) Excimer Laser-Pumped Dye Laser Facility with parameters

   332 nm - 860 nm with $0.04cm^{-1}$ bandwidth up to 20 MW peak power

4) Q-switched ruby lasers (two)

   1 J @ 694.3 nm in 20 ns pulse

5) Copper Vapor laser

   10 Watts, 2 kHz - 30 kHz, 20 - 40 ns pulse

Diagnostic Equipment

1) Optical spectrograph, with gated, intensified, optical multichannel analyzer.

2) Hammamatsu (C-1155) streak camera

3) TRW Framing camera

Oscilloscopes

1) Tektronix DSA602 Digital Signal Analyzer
2) 4 Tektronix 7844 dual beam 400 MHz oscilloscopes
3) 2 Tektronix 7904 dual channel 400 MHz oscilloscopes
4) 3 Tektronix 465 dual channel 100 MHz scopes

Curriculum Vitae

NAME: MARY L. BRAKE
Married, 3 children

PRESENT POSITION:

Associate Professor
Department of Nuclear Engineering
University of Michigan
(313) 764-1976

EDUCATION:

B.S. (With Honors, Physics), Michigan State University, 1978.
M.S. (Physics), Michigan State University, 1980.
Ph.D. (Mechanical Engineering). Michigan State University, 1983,

PROFESSIONAL POSITIONS:

Associate Professor, University of Michigan
9/90 - present
Optical diagnostics and chemical kinetic studies of glow discharges used in gas lasers and materials processing. Spectroscopic and chemical kinetic studies of intense, microsecond, electron beam interactions with low and high pressure gases and solid targets.

Assistant Professor, University of Michigan
9/84 - 9/90

Postdoctoral Scholar, University of Michigan
2/83 - 8/84

Research Assistant, Michigan State University
9/79 - 1/83

AWARDS AND SCHOLARSHIPS:
Michigan State University Alumni Scholarship
Affirmative Action Scholarship, Michigan State University

PROFESSIONAL MEMBERSHIPS:

American Physical Society
Institute of Electrical and Electronic Engineers
American Nuclear Society
American Society for Engineering Education

UNIVERSITY SERVICE:

Society of Women Engineers, Faculty Advisor (1987 - present)
Mentor for the Women in Science, H.S. summer program
Phoenix Memorial Project, Faculty Executive Committee (1988 - present)
Rackham Grant Faculty Committee (1988 - 1989)
Rackham Dissertation Grant Committee (1984)
Rackham Predoctoral Fellowship Committee (1984)
Curriculum Committee, NE Department (1987 - present)
Public Service Committee, NE Department (1988 - present)
NE Executive Committee (1985 - 1987)
President's Advisory Committee on Women's Issues (1990 - present)
University External Relations Advisory Committee (1989-present)

PROFESSIONAL ACTIVITIES:

Executive board member of the Michigan Section of the American Nuclear Society (1986-1988)
Reviewer for NSF, NSF Research Experiences for Undergraduates and Small Business Innovative Research, and AFOSR
Reviewer for Plasma Chem. and Plasma Processing, IEEE Trans. on Plasma Science, Physics Letters A, and Journal of Power and Propulsion
Member of the ANS Professional Development & Accreditation Committee (1991 -)

JOURNAL PUBLICATIONS:

1) "Observing Plasma Variations Using Plasma Induced Emission", M. Passow, T. Cotler, J. Fournier, M. Brake and M. Elta, IEEE Transactions on Semiconductor Manufacturing, to be published.

2) "Microwave Resonant Cavity Produced Air Discharges", M. Passow, M. Brake, P. Lopex, W. McColl and T. Repetti, to be published in IEEE Transactions on Plasma Science, April 1991.

3) "Chamber Material Effects on Actinometric Measurements in rf Glow Discharges", by Tina J. Cotler, Michael L. Passow, Jeffrey P. Fournier, Mary L. Brake and Michael E. Elta, J. Appl. Phys., Vol. 69, No. 5, pp. 2885-2888, 1991.

4) "Argon Ion Excitation by Relativistic Electrons: Part I. Collision Cross Sections and Deposition Efficiencies", by D. B. McGarrah and M. L. Brake, Lasers and Particle Beams 8 (3),493-506, 1990.

5) "Argon Ion Excitation by Relativistic Electrons: Part II. Chemical Kinetics", by D. B. McGarrah and M. L. Brake, Lasers and Particle Beams, 8 (3), 507-520, 1990.

6) "Optical Emission Spectroscopy of Electron Cyclotron Resonance Heated Helium Mirror Plasmas", K. Junck, M. Brake, and W. Getty, Plasma Chem. and Plasma Proc., 11 (1), 15 - 39, 1991.

7) "Production of the XeO* Excimer in a Low Power,CW Microwave Discharge", by M. Passow and M. L. Brake, Plasma Chemistry and Plasma Processing, 9, 497, 1989.

8) "Electron Temperatures of Intense Electron Beam Produced Plasmas", by M. L. Brake and T. E. Repetti, IEEE Trans. on Plasma Sci., 17(1), 60, 1989.

9) "Laser Deflection Through a Spark", C. L. Enloe, M. L. Brake, and T. E. Repetti, American Journal of Physics, 58(4), 400-403, 1990.

10) "A Theoretical and Experimental Investigation of Long Pulse, Electron Beam Produced Rare Gas Plasmas", M.L.Brake and T.E. Repetti, IEEE Trans. on Plasma Sci., 16, 581, 1988.

11) "Effects Of Electron Beam Injection on Ethylene-Air Combustion", R. Gilgenbach, S. Bidwell, R. Bosch, M. Brake, J. Tucker, T. Repetti and J. Sell, J. Appl. Phys. 62, 2553, 1987.

12) "Spectroscopic Study of Anode Plasma in a Mirosecond Electron-Beam Diode", M. Cuneo, R. Gilgenbach, and M. Brake. IEEE Transactions on Plasma Science, PS-15 375, 1987.

13) "Temporally Resolved Spectroscopy of Laser Induced Carbon Ablation Plasma", M.Brake, J. Meachum, R. Gilgenbach and W. Thornhill, IEEE Transactions on Plasma Science, PS-15, 73, 1987.

14) "Effects of Helium Upon Electron Beam Excitation of N_2^+ at 391.4 nm and 427.8 nm", M. Brake, R. Gilgenbach, R. Lucey, K. Pearce, T. Repetti, and P. Sojka, Appl.Phys Letts., 49, 696, 1986.

15) "Emission Spectroscopy of Long Pulse REB Produced Argon Plasmas", M. Brake, T. Repetti, K. Pearce, and R. Lucey J. Appl. Phys., 60 (1), 99, 1986.

16) "Spectroscopic Measurements of He_2 in the Afterglow of a Dense Z-Pinch Plasma", J. Tucker, M. Brake and R. Gilgenbach, J. Appl. Phys. 59 (6), 2251, 1986.

17) "Electron Density Measurements of Argon Surface Wave Discharges", M. Brake, J. Rogers, M. Peters, J. Asmussen and R. Kerber, Plasma Chemistry and Plasma Processing, 5, 255, 1985.

18) "Energy Deposition in Metals By Laser Guided Discharges", M. Brake, R. Gilgenbach, L. Horton, J. Tucker. Plasma Chemistry and Plasma Processing, 3, 367, 1983.

19) "Dissociation and Recombination of Oxygen Atoms Produced in a Microwave Discharge, Part I: Experiment", M. Brake, J. Hinkle, J. Asmussen, M. Hawley, and R. Kerber. Plasma Chemistry and Plasm Processing, 3, 63, 1983.

20) "Dissociation and Recombination of Oxygen Atoms Produced in a Microwave Discharge, Part II: Theoretical Calculations", M. Brake and R. Kerber, Plasma Chemistry and Plasma Processing, 3, 79, 1983.

21) "Physics in Accident Investigations", M. Brake, Physics Teacher, Volume 19, January 1981.

Ph.D. Thesis

1. Kevin Junck, "Characterization of Argon Electron-Cyclotron-Resonance-Heated Mirror Plasmas for Materials Processing", co-chair with Ward Getty, 1991.

2. Michael Passow, "Microwave, RF and Hybrid Reactor Generated Discharges for Semiconductor Processing", co - chair with M. Elta, 1991.

3. Dorothy McGarrah, "Interaction of Relativistic Electron Beams with Neutral Argon", August 1989.

4. Tom Repetti, "Emission Spectroscopy of the Interaction of a Long Pulse Relativistic Electron Beam with Rare Gases and Air", August 1989.

5. Michael Cuneo, "Characterization of the Time-Evolution of a Microsecond Electron Beam Diode with anode effect", co-chair with Prof. R. Gilgenbach, Dec. 1988.

6. John Tucker, "Electromagnetic Emissions for a Laser-Heated Z-pinch Plasma", co-chair with R. Gilgenbach, 1986.

NAME: Ronald M. Gilgenbach

BORN: December 15, 1949

Married, two children

PRESENT POSITION:
Professor
Nuclear Engineering Department and Applied Physics Program
Director, Intense Energy Beam Interaction Laboratory
The University of Michigan

EDUCATION:
Ph.D. (Electrical Eng.), Columbia University, 1978
M.S. (Electrical Eng.), University of Wisconsin, Madison, 1973
B.S. (With Honors, Electrical Eng.), University of Wisconsin, Madison, 1972

RESEARCH EXPERIENCE:
The University of Michigan:
Professor: 1989-Present
Associate Professor: 1984-1989
Assistant Professor: 1980-1984

Director, Intense Energy Beam Interaction Laboratory: 1980-Present
-Developed a major new laboratory including long-pulse electron beam accelerators and high power lasers
-Laser interactions with plasmas and materials
-Microwave heating of magnetically confined plasma
-Applications of intense laser and particle beams

JAYCOR, Alexandria, VA, 1978-1980
-Developed the first long pulse, high power (150kW),35 GHz gyrotron for plasma heating (Naval Research Laboratory)
-Performed the first definitive experiment demonstrating gyrotron electron cyclotron plasma heating in a tokamak (Oak Ridge National Laboratory)

Columbia University Plasma Laboratory, 1977-1978
-Conducted spectroscopic investigations of high power, millimeter wave radiation from intense, relativistic electron beams

Bell Laboratories, 1974-1977
-Microwave and communication engineering

OTHER RELEVANT RESEARCH EXPERIENCE:
Culham Laboratory, Abingdon, Oxfordshire, England, 1973
-Involved in laser Thomson scattering and optical plasma diagnostics with D. C. Robinson, (Summer)

University of Wisconsin Plasma Laboratory, 1972-1973
-Performed research concerning high power microwave-plasma interactions

PROFESSIONAL MEMBERSHIPS:
American Physical Society
IEEE Nuclear and Plasma Sciences Society
Sigma Xi
American Nuclear Society

HONORS AND AWARDS:
National:

1987 - Young Member Engineering Achievement Award from American Nuclear Society
1984 - Presidential Young Investigator Award
1984 - Centennial Key Award for Outstanding Young Engineer from the IEEE Nuclear and Plasma Sciences Society
1978 - Outstanding Graduate Student Award from IEEE Nuclear and Plasma Sciences Society

The University of Wisconsin:
Bergenthal Scholarship
3M Co. Scholarship
Phi Kappa Phi
Tau Beta Pi
Eta Kappa Nu
Bacon Fellowship
W.A.R.F. Fellowshi
Columbia University: Sigmi Xi

The University of Michigan: Rackham Faculty Research Grant

PUBLICATION SUMMARY:
Refereed Journal Publications: 50 published or in press
Conference Papers with Published Proceedings or Abstract: >80

PATENTS:

"Electron Beam, Ion Beam, or Neutral Particle Beam-Induced Modification or Enhancement of Combustion Reactions," Patent Number 4,885,065, Issued 1989

NATIONAL SERVICE:

Local arrangements chairman for American physical Society Division of Plasma Physics Meeting 1990
Reviewed Reports for National Research Council
Proposal Reviewer for Department of Energy
Proposal Reviewer for National Science Foundation
National Science Foundation SBIR Review Panel

UNIVERSITY ADMINISTRATIVE SERVICE:

1980-Pres	Director, Intense Energy Beam Interaction Laboratory
1988-Pres.	Faculty Senate Assembly
1987-90	Executive Board of the Rackham Graduate School
1987-89	Executive Committee of the Applied Physics Program
1987-89	Program Advisor for Engineering Physics
1986-87	College Curriculum Committee
1986-87	Executive Committee of Nuclear Engineering Department
1985-87	College Library Committee
1985-86	Search Committee for Vice President for Research

R. M. Gilgenbach

New Courses Originated

NE576: "Principles of Charged Particle Accelerators"
NE673: "Free Electron Lasers and Masers" (Taught under Topics in Theoretical Plasma Physics)

Research Results Reproduced in Books

Figure 4, Page 163 in Fusion, Vol. 1B, "Magnetic Confinement." Edited by Edward Teller.

Pages 86-89 in Plasma Heating. Published by the Physical Society of Japan. Edited by Shigeo Hagiwara, Shigetoshi Tanaka, and Atsuo Iiyoshi.

Figure 2, page 270 in Infrared and Millimeter Waves, Volume 5. Edited by K. Button.

Invited Lectures and Seminars

1) Columbia University, January 25, 1980
2) Yale University, April 24, 1980
3) The University of Wisconsin, April 28, 1980
4) Massachusetts Institute of Technology, May 2, 1980
5) Lawrence Livermore Laboratory, May 9, 1980
6) Naval Research Labs, January 19, 1983
7) The University of Wisconsin, March 14, 1983
8) Calvin College, November 16, 1982
9) Oakland Community College, February 24, 1983
10) General Motors Research Labs, October 18, 1983
11) Michigan Technology Council, September 18, 1984
12) Columbia University, March 22, 1985
13) Los Alamos National Laboratory, May 24, 1985
14) Oak Ridge National Laboratory, December 16, 1986
15) Sandia National Laboratory, April 6, 1987
16) Air Force Weapons Laboratory, August 7, 1987
17) Naval Research Laboratory, February 23, 1988
18) Sandia National Laboratory, August 11, 1988
19) Los Alamos National Laboratory, April 17, 1989
20) Air Force Weapons Laboratory, April 18, 1989
21) Los Alamos National Laboratory, May 24, 1990
22) University of Maryland. March 15, 1991
23) Lawrence Livermore National Lab, May 8, 1991

Refereed Papers for the Following Scholarly Journals

1) Nuclear Fusion
2) The Physics of Fluids
3) Nuclear Technology/Fusion
4) IEEE Transactions on Plasma Science
5) Journal of American Industrial Hygiene Association
6) Plasma Chemistry and Plasma Processing

R.M. Gilgenbach

Doctoral Committee Chairmanships

1) Paul Weber, "A Study of the 10cm Duopigatron as a Source of Intermediate and High Mass Particle Beams,"(Defended March 19, 1984). Employed at Lawrence Livermore National Lab

2) Lorne Horton, "Hydrodynamics of Gas Channels Formed by Lasers and Guided Discharges," (Defended March 20, 1985); Employed at Oak Ridge National Lab

3) John Booske, "Electron Cyclotron Heating and Emission in Magnetic Mirror Confined Plasma," (Defended July 30, 1985) Employed at University of Wisconsin

4) John Tucker, "Electromagnetic Emissions from a CO_2 Laser Heated Z-Pinch Plasma," (Defended March 28, 1986), Co-chair with M. L. Brake; Employed at Naval Research Lab

5) Ronnie Shepherd, "Dynamics and Resistivity of Plasmas Formed by Capillary Discharges," (Defended May 22, 1987); Employed at Lawrence Livermore National Lab

6) Robert Lucey, "Generation and Ion Focused Regime Propagation of Long Pulse Relativistic Electron Beams," (Defended January 28, 1988); Employed at MIT Lincoln Lab

7) Carl Lon Enloe, "Ultraviolet Induced Flashover of Highly Angled Polymeric Insulators in Vacuum," (Defended February 12, 1988); Employed at Air Force Geophysics Lab

8) Joseph Meachum, "Neutral Beam Interactions with Laser Ablation Plasmas," (Defended September 23, 1988); Employed at Physics International

9) M. Cuneo, "Visible and Ultraviolet Spectroscopy of Anode Plasmas in Microsecond Electron Beam Diodes," Co-Chair with M. L. Brake (Defended December 20, 1988); Employed at Sandia National Lab

10) S. Bidwell, "Long Pulse Electron Beam Interactions with Gases and Flames," (Defended January 26, 1989); Employed at University of Maryland

11) J. D. Miller, "Transport and Stability of Long Pulse High Current Electron Beams in Ion-Focused Regime Plasma";

Channels," (Defended June 1, 1989); Employed at Naval Surface Warfare Center

12) D. Whaley, "Highly Charged Ions from a Magnetic Mirror" Co-chair with Getty (Defended May 11, 1989); Employed at Ecole Polytechnique Federale de Lausanne

13) J. G. Wang, "Cyclotron Autoresonance Maser Driven by a Long-Pulse Intense Electron Beam" (Defended June 1, 1989); Employed at University of Maryland

14) P.L.G. Ventzek, "The Hydrodynamics of Excimer Laser Alation Processing of Materials in Vacuum and Gases" (defended March 11, 1991); Postdoctoral Scholar At University of Michigan

15) T. A. Spencer, "High Power, Long Pulse Gyrotron-Backward-Wave-Oscillator Experiments", (defended May 15, 1991); Postdoctoral Scholar At University of Michigan

16) J. J. Choi, "Bragg-Resonator Cyclotron Masers Driven By Intense, Microsecond Electron Beam Accelerator", (defended April 30, 1991); Employed at Naval Research Laboratory

REFEREED JOURNAL PUBLICATIONS OF R. M. GILGENBACH

50) "Measurement of Relativistic Electron Beam Perpendicular-to-Parallel Velocity Ratio by Cerenkov Emision and Radiation Darkening on a Glass Plate", J.J. Choi, R. M. Gilgenbach, T.A. Spencer, P. Menge, and C.H. Ching, Rev. Sci. Inst., Accepted for publication

49) "Deflection of Carbon Dioxide laser and Helium Neon Laser Beams in a Long-Pulse Relativistic Electron Beam Diode", R. A. Bosch, H. Ching, R. M. Gilgenbach, P.L.G. Ventzek, P.R. Menge, J.J. Choi, and T.A. Spencer, Review of Scientific Instruments,in press for July 1991 issue

48) "Laser Beam Deflection Measurements and Modeling of Pulsed Laser Ablation Rate and Near-Surface Atom Densities in Vacuum", P.L.G. Ventzek, R. M. Gilgenbach, J. A. Sell, and D. Heffelfinger, Journal of Applied Physics, July 15, 1991

47) "Dynamics of Excimer Laser-Ablated Aluminum-Neutral-Atom Plume Measured by Dye-Laser-Resonance-Absorption Photography", R. M. Gilgenbach and P.L.G. Ventzek, Applied Physics Letters, 58 1597 (1991)

46) "The Effect of X-Y Coupling on the Beam-Breakup Instability", R.A. Bosch and R. M. Gilgenbach, Applied Physics Letters, 58 699 (1991)

45) "Photothermal and Photoacoustic Beam Deflection as a Probe of Laser Ablation of Materials", J. A. Sell, D. Heffelfinger, P.L.G. Ventzek, and R. M. Gilgenbach, Journal of Applied Physics, 69 1330 (1991)

44) "Schlieren Measurements of the Hydrodynamics of Excimer Laser Ablation of Polymers in Atmospheric Pressure Gas," P.L.G. Ventzek, R. M. Gilgenbach, J. Sell, and D. Heffelfinger, Journal of Applied Physics, Journal of Applied Physics, 68 965 (1990)

43) "Transport of Long-Pulse, High Current Electron Beams in Preformed Monatomic Plasma Channels in the Ion Focus Regime," J. D. Miller and R. M. Gilgenbach, IEEE Trans. Plasma Science, 18 658 (1990).

42) "Laser Beam Deflection as a Probe of Laser Ablation of Materials,' J. Sell, D. Heffelfinger, P. Ventzek, and R. M. Gilgenbach, Applied Physics Letters, 55 2435 (1989)

41) "Frequency-Tunable, High Power Microwave Emission from Cyclotron Autoresonance Maser Oscillation and Gyrotron Interactions," J. G. Wang, R. M. Gilgenbach, J. J. Choi, C. A. Outten, and T. Spencer, IEEE Trans. Plasma Sci. 17 906 (1989).

40) "Spectroscopic Observations of UV-Laser-Induced Flashover across an Angled Insulator," C. L. Enloe and R. M. Gilgenbach, IEEE Trans. on Plasma Science, 17, 550 (1989).

39) "Electron Beam Induced Acoustic Wave Enhancement of Gaseous Combustion," with S. W. Bidwell and R. A. Bosch, Journal of Applied Physics, 65, 782 (1989).

38) "Transport and Stability of Long-Pulse Relativistic Electron Beams in UV Laser Induced Ion Channels," with R. F. Lucey, J. D. Miller, J. E. Tucker, and R. A. Bosch, The Physics of Fluids B, 1 430 (1989).

37) "Propagation of Microsecond Electron Beams in Gases and Excimer Laser-Ionized Channels in the Ion-Focused Regime," with R. F. Lucey, J. E. Tucker, and C. L. Enloe, Laser and Particle Beams, 6 687 (1988).

36) "Undulation of a Magnetized Electron Beam by a Periodic Ion Channel," with R. A. Bosch, The Physics of Fluids, 31 3127 (1988).

35) "Current Clamping in Long Pulse Electron Beam-Gas Interactions," with R. A. Bosch and S. W. Bidwell, IEEE Trans. on Plasma Science, 16, 428 (1988).

34) "Influence of Damping on the Ion Hose Instability", with R.A. Bosch, The Physics of Fluids, 31, 2006 (1988).

33) "Microscopic and Macroscopic Material Properties Effects on Ultraviolet-Laser-Induced Flashover of Angled Insulators in Vacuum," with C. L. Enloe, IEEE Trans. on Plasma Science, 16, 379 (1988).

32) "Radial Oscillations and the Ion Hose Instability of an Electron Beam Propagating in a Periodic Ion Channel," with R. A. Bosch, The Physics of Fluids, 31, 634 (1988).

31) "Leak Widths Resulting from Plasma Diffusion in a Magnetic Cusp", with R.A. Bosch, Physics Letters A, 128, 437, (1988).

30) "Low Voltage Models of Particle Accelerator Circuits," American Journal of Physics, 56, 822 (1988).

29) "Transport and Modulation of Relativistic Electron Beams by

Periodic Ion Channels," with J. Miller, The Physics of Fluids, 30 3165 (1987).

28) "Fast, Sensitive Laser Deflection System Suitable for Transient Plasma Analysis," with C. L. Enloe, Review of Scientific Instruments, 58, 1597 (1987).

27) "Effects of Electron Beam Injection on Ethylene-Air Combustion," with S. Bidwell and R. Bosch et al., Journal of Applied Physics, 62 2553 (1987).

26) "Spectroscopic Study of Anode Plasma in a Microsecond Electron Beam Diode," with M. E. Cuneo and M. L. Brake IEEE Trans. on Plasma Science, PS-15 375 (1987).

25) "Soft X-Ray Emission from a CO_2 Laser Heated Z-Pinch Plasma," with J. E. Tucker, Plasma Chemistry and Plasma Processing, Vol. 7, 365, (1987).

24) "Ultraviolet-Induced Flashover of a Plastic Insulator Using a Pulsed Excimer Laser," with C. L. Enloe, Plasma Chemistry and Plasma Processing, 7, 89 (1987).

23) "Temporally Resolved Spectroscopy of Laser Induced Carbon Ablation Plasmas," with M. L. Brake, J. Meachum, and W. Thornhill, IEEE Trans. on Plasma Science, PS-15, 73 (1987).

22) "Amorphous Alloys Formed by Microsecond Current Pulses," with B. M. Clemens and S. Bidwell, Applied Physics Letters, 50, 495 (1987).

21) "Effects of Helium Upon Electron Beam Excitation of N2+ at 391.4 nm and 427.8 nm," with M. L. Brake, T. Repetti, and K. Pearce, Applied Physics Letters, 49, 696 (1986).

20) "Extended Frequency Compensation of a Diamagnetic Loop," with J. H. Booske and W. D. Getty, Plasma Physics and Controlled Fusion, 28 1449 (1986).

19) "X-Ray Measurements During Whistler Mode Electron Cyclotron Resonance Plasma Startup and Heating in an Axisymmetric Magnetic Mirror," with J. H. Booske, W. D. Getty, T. P. Goodman, and J. E. Pitcher, IEEE Transactions on Plasma Science, PS-14, p. 592 (1986).

18) Spectroscopic Measurements of He_2 in the Afterglow of a Dense Helium Z-Pinch Plasma," with J. E. Tucker and M. L. Brake, Journal of Applied Physics, 59, 2251 (1986).

17) "Amorphous Alloys from Microsecond Current Pulses," with B. Clemens, J. Bucholz, and S. Bidwell, Festschrift of the Turnbull Symposium, Published by the Materials Research Society (1985).

16) "Experiments on Whistler Mode ECRH Plasma Startup and Heating in an Axisymmetric Magnetic Mirror," with J. H. Booske and W. D. Getty, The Physics of Fluids, 28, 3116 (1985).

15) "Intermediate and High Mass Beams from a 10 cm Duopigatron Ion Source," with P. D. Weber, Plasma Chemistry and Plasma Processing, 4, 75 (1984).

14) "Microwave-Plasma Interaction Experiment," American Journal of Physics, 52, 710 (1984).

13) "Mirror-Electrode for Laser Initiated Discharge Channels," with L. D. Horton, Review of Scientific Instruments, 55, 503 (1984).

12) "Collinear Investigation of Laser Initiated Reduced Density Channels," with L. D. Horton, Applied Physics Letters, 43, 1010 (1983).

11) "Energy Deposition in Metals by Laser Guided Discharges," with M. L. Brake, L. D. Horton, and J. E. Tucker, Plasma Chemistry and Plasma Processing, 3, 367 (1983).

10) "Effects of Gamma Emission on Laser Ionized Plasma Channels for ICF Reactors," with L. D. Horton and O. E. Ulrich, Nuclear Technology/Fusion 4, 508 (1983).

9) "Localized Metallic Melting and Hole Boring by Laser Guided Discharges," with O. E. Ulrich and L. D. Horton, The Review of Scientific Instruments, 54, 109 (1983).

8) "Boundary Effects on the Dynamics of Channels Generated by Laser Initiated Discharges," with L. D. Horton, The Physics of Fluids, 25, 1702 (1982).

7) "Electron Cyclotron/Upper Hybrid Resonant Preionization in the ISX-B Tokamak," (with M. E. Read, K. E. Hackett, R. F.Lucey, V. L. Granatstein, A. C. England, C. M. Loring, J. B. Wilgen, R. C. Isler, Y-K. M. Peng, K. H. Burrell, O. C. Eldridge, M. P. Hacker, P. W. King, A. G. Kulchar, M. Murakami, and R. K. Richards), Nuclear Fusion 21, 319 (1981).

6) "Spatial and Temporal Coherence of a 35-GHz Gyromonotron Using the TE01 Circular Mode," (with M. E. Read,

R. F. Lucey, Jr., K. R. Chu, A. T. Drobot, and V. L. Granatstein), IEEE Trans. on Microwave Theory and Techniques, MTT-28, 875 (1980).

5) "Heating at the Electron Cyclotron Frequency in the ISX-B Tokamak," (with M. E. Read, K. E. Hackett, R. Lucey, B. Hui, V. L. Granatstein, K. R. Chu, A. C. England, C. M. Loring, O. C. Eldridge, H. C. Howe, A. G. Kulchar, E. Lazarus, M. Murakami, and J. B. Wilgen), Physical Review Letters, 44, 647 (1980).

4) "Cyclotron Harmonic Damping in Stimulated Raman Scattering from an Intense Relativistic Electron Beam," (with T. C. Marshall and S. P. Schlesinger), The Physics of Fluids, 22, 1219 (1979).

3) "Spectral Properties of Stimulated Raman Radiation from an Intense Relativistic Electron Beam," (with T. C. Marshall and S. P. Schlesinger), The Physics of Fluids, 22, 971 (1979).

2) "Thermal Paper as a Diagnostic for Intense Relativistic Electron Beam Dynamics," (with T. C. Marshall and D. B. McDermott), The Review of Scientific Instruments, 49, 1098 (1978).

1) "Microwave Heating Rates for a Plasma in a DC Magnetic Field as Determined from Inverse Synchrotron Emission," (with J. L. Shohet), Nuclear Fusion, 14, (1974).

Reprints removed

END

DATE
FILMED
2/11/94